Partial Molar Properties of Aqueous Monosaccharide Solutions at Elevated Pressure

Asbjørn Aarflot
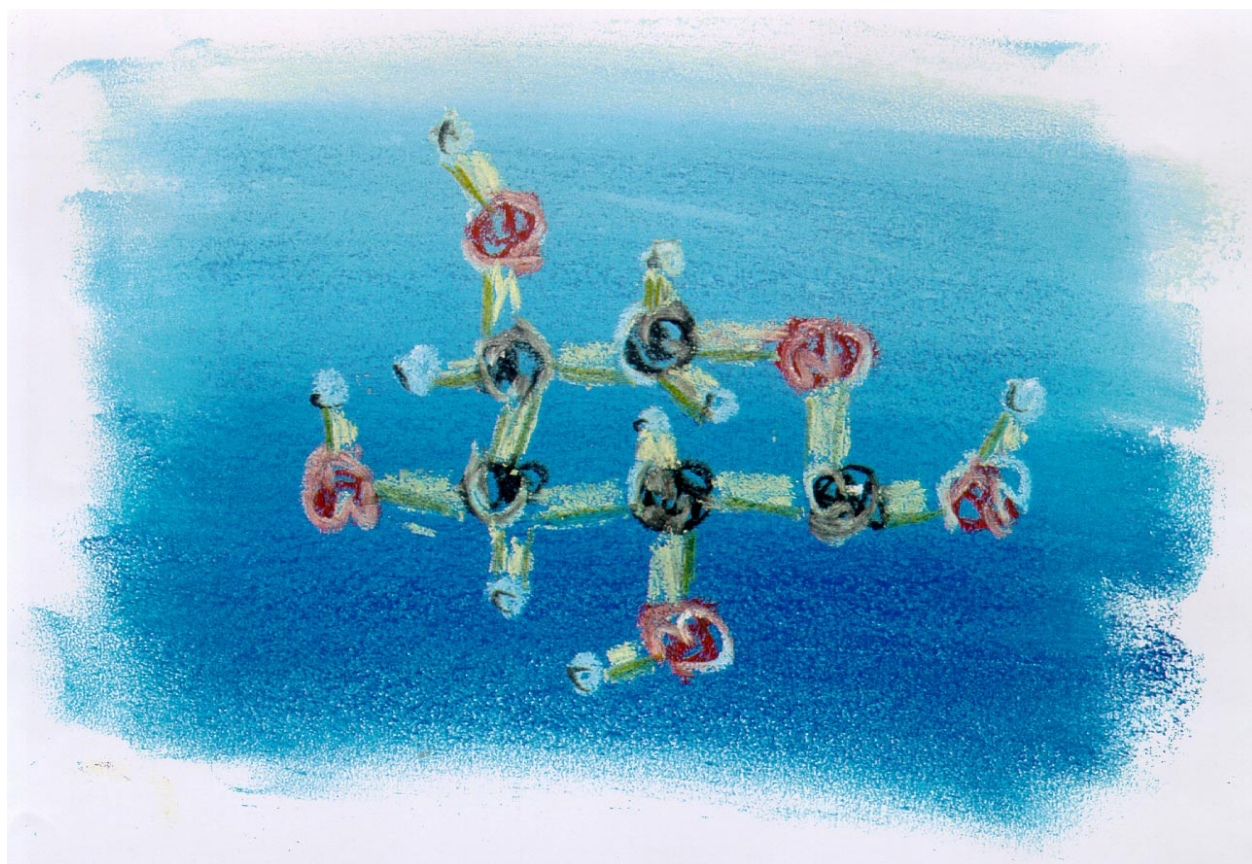
Forord

Arbeidet med denne hovudfagsoppgåva tok til våren 1999 ved Kjemisk Institutt, Universitetet i Bergen under rettleiing av Professor Harald Høiland. Alle målingar er utført ved Kjemisk Institutt, Universitet i Bergen, avdeling for fysikalsk kjemi.

Det har vore ei særs interessant tid her ved Kjemisk Institutt. Det har aldri vore mangel på utfordringar. Særleg utfordrande var det å setja i saman trykkapparaturen og få denne til å gi tilfredsstillande resultat.

Eg vil gjerne takka Professor Harald Høiland for fruktbare og lærerike diskusjonar og god fagleg rettleiing. Spesielt vil eg takka for studieturen til Leeds som var veldig inspirerande.

Ein takk vert også retta til overingeniør Einar Høgseth og avdelingsingeniør Steinar Vatne som alltid har vore hjelpsame når apparatur og instrument svikta.

Medstudentane her ved instituttet i alle etasjar, har gjort studietida her til ei minnerik tid. Særleg vil eg takka gutane i Nanzy Boyz for gode pasningar og frie diskusjonar. Eg vil også takka Øystein Strand og Rita Skålevik for fruktbare diskusjonar og hjelp til utrekning og bruk av apparatur.

Eg vil også takka Ann-Kristin Strømmen for den flotte illustrasjonen av α-L-arabinose.

Til slutt vil eg takka familien min for veldig god støtte under arbeidet.

Bergen, 15. mars 2001

Asbjørn Aarflot

Summary

Limiting partial molar volume, V_2^∞, limiting partial isothermal and isentropic molar compression, $K_{T,2}^\infty$, hydration number, n_H, and pressure derivative of $K_{T,2}^\infty$ for D-glucose, D-galactose, D-mannose, D-ribose and L-arabinose in aqueous solutions are presented at pressures ranging from 1 to 1400 bars. These have been acquired by means of speed of sound measurements at 1-1400 bars, density measurements at atmospheric pressure and calculation of apparent molar properties. Properties at elevated pressure were calculated using an iterative method, which require knowledge of expansivity, α, and volume specific heat capacity, σ_p. Knowledge of α and σ_p makes it possible to calculate the thermodynamic true apparent isentropic molar compression $K_{S,\phi,2}$. The difference between true and practical $K_{S,\phi,2}$ was found to be insignificant for the given concentration range, 0,06-0,15 molal.

The obtained results reveal information about hydration of the investigated carbohydrates as pressure rise. As pressure rise there is a substantial increase in $K_{T,2}^\infty$, which indicate altered hydration. A diminishing difference in $K_{T,2}^\infty$ with increasing pressure suggests less stereo-specific hydration at high pressures.

$K_{2,T}^\infty$ is negative at all measured pressures for all the investigated monosaccharides except for D-mannose and D-ribose which are zero at 1400 bar and 1100 bar, respectively, and positive at higher pressures. An interpretation of the physical meaning of zero partial isothermal molar compression is given.

Table of contents

1 Introduction

Carbohydrates constitute an important class of biological molecules. They are important in numerous processes such as energy storage, cold- and drought-resistance[1] and molecular recognition. Of industrial applications it is worth mentioning non-ionic surfactants, the ability to form amorphous glassy solids[2] and of course food. Now what is it that makes a class of molecules to have such impressive wide variety of uses? The answer can be found in water. Or more specifically, in their interaction with water.

1.1 Carbohydrates

The group of carbohydrates can be divided into three subgroups: monosaccharides, oligosaccharides and polysaccharides. Ordinary table sugar, sucrose, is a disaccharide; that is, it is made out of two monosaccharides, and hence comprises under the group of oligosaccharides. Starch and cellulose are examples of polysaccharides. Among monosaccharides are glucose, or grape sugar and fructose. Monosaccharides are then divided into groups of number of carbon-atoms, hexoses and pentoses, and whether the functional group is an aldehyde or ketone, aldohexoses and ketohexoses.

1.1.1 Stereochemistry and nomenclature

Monosaccharides can be viewed as polyhydroxylaldehydes or polyhydroxylketones with formula $C_nH_{2n}O_n$, where n is 5 or 6. This implies several chiral carbon-atoms and it is this chirality that differ carbohydrates in the same group.

1.1.1.1 The D/L system

Each monosaccharide has an optical stereoisomer that rotates the plane of polarised light in opposite direction and that is superimposeable on the other. A monosaccharide is designated D or L depending on its structural resemblance to D- or L-glyceraldehyde. D- glyceraldehyde is defined as the optical isomer that rotates the plane of polarised light in a clockwise (+) angle of rotation and for L-glyceraldehyde the opposite. There is, however, no link between +/- rotation of plane of polarised light and D/L for other than glyceraldehyde[3]. D/L of other monosaccharides are set to D if the hydroxyl-group furthest away from the most oxidised group is drawn to the right in a Fisher-projection and L if the same group is drawn to the left. Two pairs of optical isomers are drawn in Fischer-projections in Figure 1.
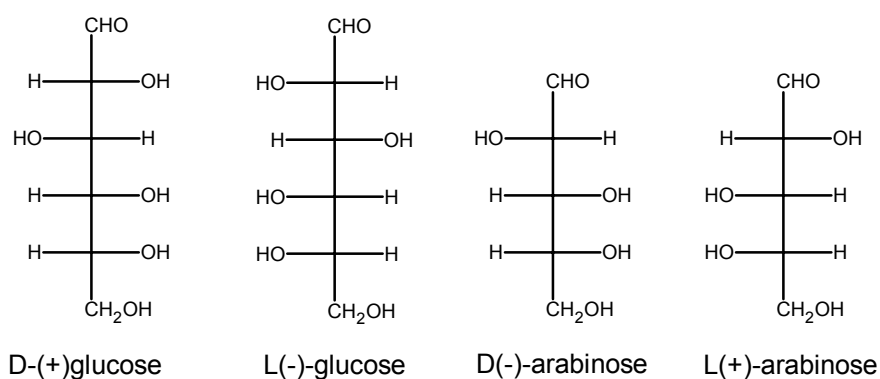
Figure 1   Designation of D and L for monosaccharides.

Most natural carbohydrates are D-carbohydrates, but arabinose appears naturally as both L-and D-arabinose[4].

1.1.1.2 Cyclic carbohydrates.

Pentoses and hexoses in aqueous solution form six- (pyranoid) and/or five- (furanoid) membered hemiacetal ring structures trough an intramolecular reaction. The ring formation generates a new asymmetrical carbon atom at C-1, the anomeric centre, thereby giving rise to diasteroisomeric hemiacetals which are called anomers and labelled α and β. The original designation of α and β is a related to the configuration of at the anomeric centre correlated to that of the highest-numbered asymetric centre of the sugar. A more convenient way is to use Haworth formulae (See Figure 2). All D-sugars are designated α if the hydroxyl-group at the anomeric centre projects downwards and β if it projects upwards. For L-sugars the opposite counts.

α-D-arabinofuranose   α-D-arabinopyranose   α-L-arabinopyranose   α-L-arabinopyranose

α-D-glucofuranose   α-D-glucopyranose   α-L-glucopyranose   α-L-glucopyranose
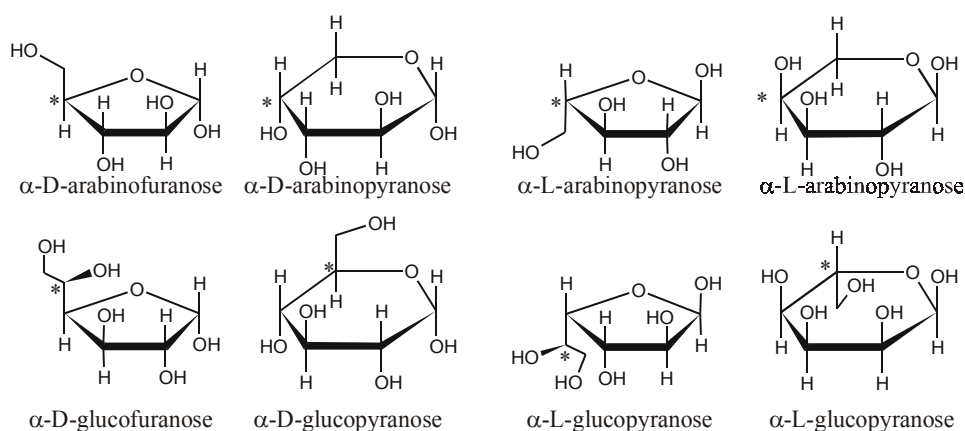
Figure 2   Anomeric configuration of D-glucose and L-arabinose in Haworth formulae. Asterisks denote the last asymmetric centres of the configurations of which determine the D- or L-assignments and serve as a reference for α- and β-assignments. Note that these configurations do not necessarily represent the most stable conformer.

1.1.1.3 Conformation of pyranoid carbohydrates

Unlike cyclohexane, where the two possible chair conformers are indistinguishable, the chair conformations of pyranoid structures of carbohydrates are enantiomers[4]. The two different conformations are called $^4C_1$ and $^1C_4$ depending on the relative orientation of C1 and C2. $^1C_4$ is also sometimes referred to as inverted chair conformation. A reference plane is selected which contains the maximum number of ring atoms, and the lowest numbered carbon atom is chosen as an exoplanar atom. The exoplanar atom projecting outwards towards the viewer from the plane when viewed with clockwise numbering is superscript (Figure 3).   Table 1 lists the preferred conformation of various sugars. For D-sugars the $^4C_1$ conformation is the most abundant although D-arabinose in large exist as α-D-arabinopyranose in the $^1C_4$ conformation.

I   **II**   **III**

$^4C_1$ $^4C_1$ $^1C_4$
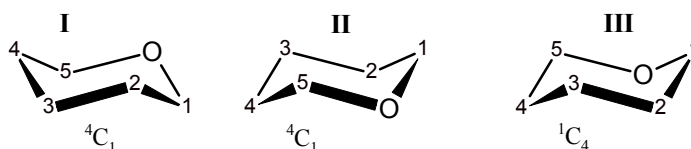
Figure 3 $^4C_1$ and $^1C_4$ labelling of pyranoses.

1.1.2 Complex mutarotation

Often the difference in free energy between the various forms of one sugar are small so that, under suitable conditions, two or more of the structurally distinct species can coexist in equillibrium[5]. The equilibrium reactions of monosaccharides are referred to as complex mutarotation. Figure 4 shows complex mutarotation for D-glucose.
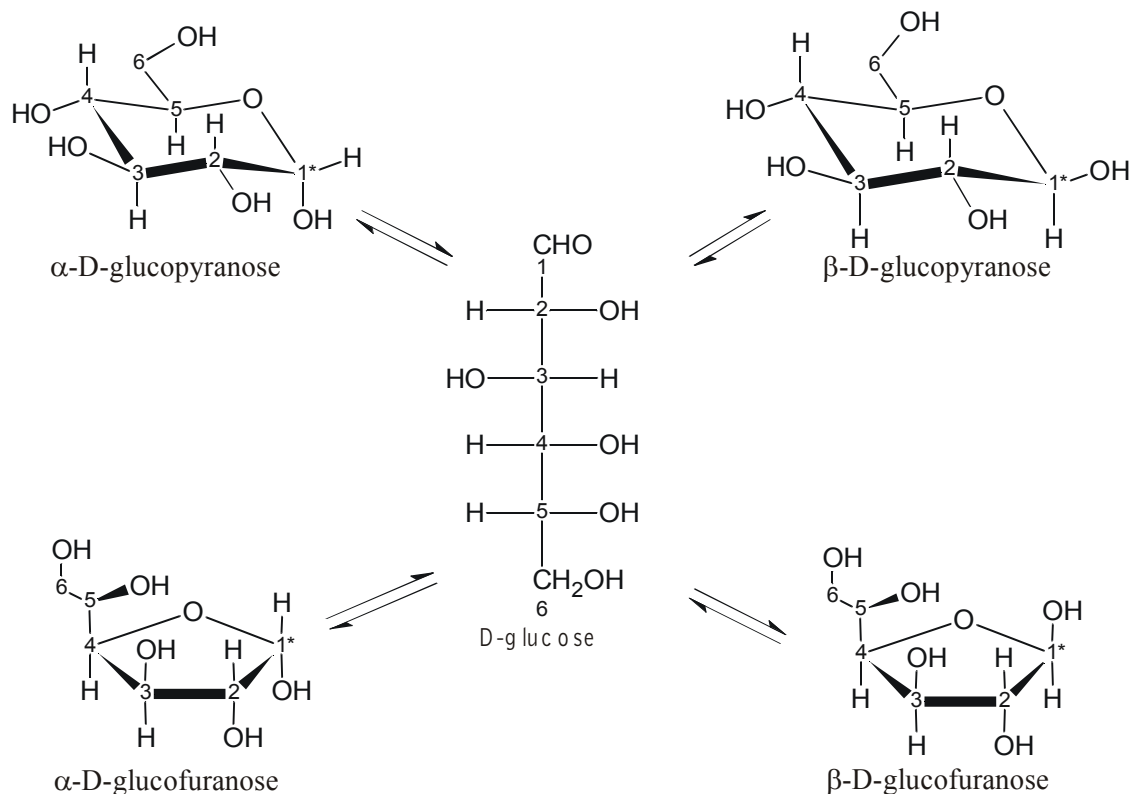
Figure 4   Complex mutarotation of D-glucose in water. Asterisks denote the anomeric centres in cyclic structures.

Table 1   Proportion (%) of pyranose and furanose forms aldoses at equilibrium in deuterium oxide solution.

Aldose	T	α-pyranose		β-pyranose		α-furanose	β-furanose	Conf. of dom. conformer[g]
		($^4C_1$)	($^1C_4$)	($^4C_1$)	($^1C_4$)			
D-glucose[a]	35°C	35	-	65	-	-	-	1e2e3e4e6e
D-galactose[b]	31°C	29		64		3	4	1e2e3e4a6e
D-mannose[b]	44°C	65,5		34,5		-	-	1a2a3e4e6e
D-ribose[a]	30°C	23	-	41	14	8	14	1e2e3a4e
D-arabinose[b]	31°C		60	35		2,5	2	1e2e3e4a
L-arabinose[c]	-	63[d,e]	e	37[d,f]		low	low	1e2e3e4a

[a] Ref. 6, [b] Ref. 7,8 this reference does not give proportions of ($^4C_1$) and ($^1C_4$) but state the most dominant chair conformation of α- and β- pyranose. [c] Ref. 9, [d] Relative to total amount of L-arabinopyranose. [e] ($^4C_1$) is assumed to be the most dominant conformer of α-L-arabinopyranose due to three equatorial hydroxyl groups. [f]Both ($^4C_1$) and ($^1C_4$) is assumed to be present in equal amounts. [g] e and a designate the numbered hydroxyl groups as equatorial or axial, respectively.

Table 1 lists equilibrium compositions of various monosaccharides in deuterium oxide. The most stable conformer in crystalline form is often not the most stable conformer in aqueous

solutions. In crystalline form the conformation are solely determined by intramolecular energies. The dominant form of aldopentoses and aldohexoses is either the α- or the β-anomer of the pyranose[7].

The equilibrium composition have been found to be dependent on temperature[10,11], but a study on D-glucose suggest that it is not altered as function of pressure[12].

1.2 Solute solvent interactions

When a solute molecule is in an aqueous environment, its functional groups must interact with the inherent structural requirements of the solvent water. Its presence can impose an alternate structuring-pattern on the adjacent water molecules. Such solvent structuring is often invoked explain the properties of aqueous solutions[13]. A fundamental understanding of solute-solvent interactions in a given system is of vital importance when studying molecular recognition, taste, reaction kinetics, micellar systems etc.

With water as solvent, solute-solvent interactions is often referred to as hydration. Depending on the solute one can have hydrophobic ("water-rejecting") and hydrophilic ("water-loving") hydration. Hydrophobic hydration is less site-specific whilst hydrophilic hydration of polar groups is very site-specific.

There exist a wide variety of techniques to probe hydration effects. NMR, Dielectric Relaxation, volumetric and densimetric analysis, ultrasonic analysis and molecular dynamics simulations, MD. Common for them all is that they can give information about the hydration layer, that is, water structuring to a solute molecule.

1.2.1 Van der Waals volume and partial molar volume

Partial molar volume, V_2, is a useful property to study solute-solvent effects. Generally one can say that V_2 is the difference in volume that occur when one mole of solute is added to a solvent so that this become an ideal solution. An ideal solution is a solution where solute-solute interactions are absent. This is rarely true for real solutions and it therefore often more convenient to use limiting partial molar volume, V_2^∞, where V_2 is extrapolated to zero concentration.

Edwards and Farrell[14] suggested in 1975 a relation between partial molar volume and the van der Waals volume. The solute molecules are treated as a sphere with van der Waals radius r_w.

Equation 1
$$V_2 = \frac{4}{3}\pi(r_w + \Delta)^3$$

which was later modified by Shahidi, Farrell and Edwards[15] to

Equation 2
$$V_2 = \frac{4}{3}\pi(r_w + \Delta)^3 - n\sigma$$

where V_2 is the partial molar volume, r_w is the van der Waals radius, Δ is the void volume separating a solute and a solvent molecule, n is number of hydrophilic groups and σ is decreased volume. The calculated partial molar volumes were consistent with available experimental data. However, this model and other models based on an additive approach[16]

give stereoisomers equal partial molar volume. It is therefore not suited to explain the difference in hydration of carbohydrates[17].

1.2.2 Partial molar compression and the intrinsic volume approach

The partial molar volume may be divided in an intrinsic part V_w and an empty volume part V_e associated with the packing of the solvent molecules around the solute[18].

Equation 3 $$V_2 = V_w + V_e$$

V_w is by far the largest contributor to the partial molar volume. The V_e term contains all effects due to solute-solvent interactions including H-bonding, solvent shrinkage, electrostriction, hydrophobic and hydrophilic hydration, and long-range effects on the water structure[16,19]. Due to the intrinsic contribution to V_2 is difficult to obtain information in stereo specific hydration. One can assume that the intrinsic volume is more or less incompressible compared to the empty volume part. Hence the pressure derivative of partial molar volume contains information about the solute-solvent interactions[18].

The negative pressure derivative of partial molar volume is often referred to as the partial molar compressibility, but this work will adopt the notation of Blandamer[20,21] and hence recognise it as partial molar compression, $K_{T,2}$. The definition and calculation of $K_{T,2}$ and other related thermodynamic properties are given in chapter 2 at page 10.

A negative $K_{T,2}$ imply that the partial molar volume, and thereof V_e, increase as function of pressure. Pure water has a molar compression of $8,17 \cdot 10^4$ $cm^3mol^{-1}bar^{-1}$. In the case of hydration of an apolar hydrophobic solute, the water molecules in the hydration layer will form stronger hydrogen bonds to each other (hydrophobic hydration) and therefore the hydration layer will be less compressible than pure water. Consequently, a slightly negative limiting compression per methylene group is found. When ions are introduced into water they usually break the water structure by electrostiction. Water around ions is dense and less compressible than bulk water, leading to typically large negative molar compression $((-30 \text{ to } -50) \cdot 10^4$ $cm^3mol^{-1}bar^{-1}$. The partial molar compression carbohydrates have intermediate values. This suggests that the hydrogen-bonded structure of water is only slightly disturbed by the presence of a carbohydrate molecule[22].

1.3 Hydration models

Aqueous sugar solutions were long thought to be ideal solutions. To make a simple model of the hydration seemed to be difficult[23]. Even so it is of vital importance to obtain such a model because of the biological importance of carbohydrates and macromolecules with carbohydrate constituent parts.

1.3.1 Early hydration models

In 1958 Kabayama and Patterson[24,25] studied mutarotation of D-glucose and suggested a model where β-D-glucopyranose and β-D-xylopyranose could align into a hexagonal (tridymite) water structure similar to that of ice. It was pointed out that from this view it was favourable to have an equatorial hydroxyl group at the anomeric centre although the axial position is favoured in the crystalline state.

In 1972 Franks and Suggett [26,19] introduced a model later called the stereo specific hydration model. It was proposed that the number of equatorial hydroxyl groups present in the carbohydrate molecule would determine carbohydrate hydration. This model was based on the fact that β-D-glucose anomer is predominantly present in water and that it would fit better into a three-dimensional hydrogen-bond network of water than α-D-glucose does. To explain why equatorial hydroxyl-groups were favoured they compared the distance between the next nearest neighbour oxygen in water and sugar. Warner[27] had previously found the distance between next-nearest oxygens in a monosaccharide with all equatorial hydroxyl-groups to be 4,86 Å. This was approximately the same as the distance in water, 4,90 Å. The model gained support from later work[28,29,30]. The stereo specific hydration model was not able to explain differences in partial molar compression[18]. A better way seemed to include the relative positions of the hydroxyl-groups. The model could also not explain the long-range effects of anisotropic solvent structuring induced by a carbohydrate found by molecular dynamics simulations[13].

1.3.2 The modified stereo specific hydration model

Galema et.al[31,32] found retardation for the hydration of 1-benzoyl-3-phenyl-1,2,4-triazol in a carbohydrate solution. The retardation was stereo specific and it was assumed that this effect, induced by carbohydrates, originated from hydration sphere overlap effects[33]. G(C) values, which is representative of the interaction between the carbohydrate and the initial state and activated complex for the hydrolysis reaction, were measured. A carbohydrate with little effect on the hydration would have a low G(C) value; that is large and negative. The experiments showed that G(C) was dependent on the relative position of OH(2) and OH(4) (See Figure 5 for numbering of hydroxyl-groups) Both OH(2) and OH(4) axial gave the most negative G(C) value and hence the best compatibility with water. OH(2) equatorial and OH(4) gave less negative values and thereof had the poorest compatibility with water.

Hydration numbers obtained from compressibility studies showed the same results[22]. Carbohydrates with both OH(2) and OH(4) axial had a lower hydration number and higher partial molar compression (Galema: compressibility) than if OH(2) were equatorial and OH(4) axial. In another study partial molar heat capacity was found not to be sensitive enough to characterise differences in hydration of carbohydrates due to a large intrinsic contribution[34].
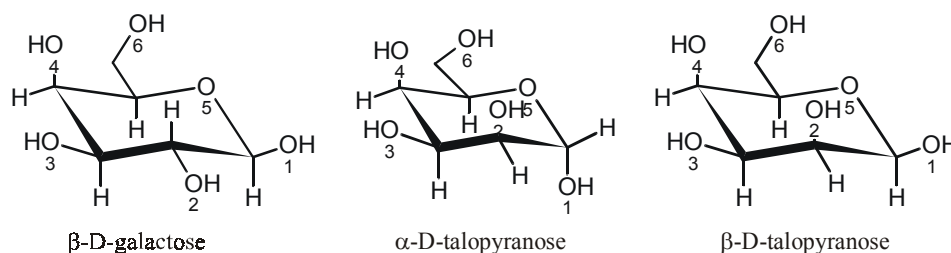
Figure 5   Hydroxyl group numbering in modified stereo specific hydration model

Molecular dynamics, MD, simulations gave further insight to the stereo specific hydration[35]. It was found that for both α- and β-D-talopyranose the distances in the O_2-O_4-O_5 were comparable to the nearest and next-nearest oxygen distances in water. This was not the case for β-galactopyranose. Only the O_4-O_5 distance was comparable to those of water. The O_1-O_3-O_6 plane of both α- and β-D-talopyranose made reasonably good fit for all three distances whilst only two for β-D-galactopyranose did so. The average number of hydrogen bonds in water and between oxygen in the carbohydrate and water were also calculated. They showed that there was a decrease in water-water hydrogen bonding with the largest for β-D-

galactopyranose. β-D-galactopyranose also made the most hydrogen bonds to water. For both α- and β-D-talopyranose there were a significant drop in bonding between O_2-water and O_4-water which suggested an intramolecular hydrogen bond. Galema coined this model the modified stereo specific hydration model. A summary is given in Table 2.

Table 2   The modified stereo specific hydration model

	Group 1	Group 2	Group 3
OH(2)	axial	axial or equatorial	equatorial
OH(4)	axial	equatorial	axial
G(C)	large and negative	intermediate large negative	small negative
$K_{S,2}^{\infty}$ and $K_{T,2}^{\infty}$	Negative and close to water	Intermediate negative	Negative and lower than that of group 1 and 2
Fit to water	Very good	Intermediate good	not good compared to 1 and 2

1.3.3 Molecular dynamics simulations

In recent years there has been an increase in molecular dynamics, MD, simulations of simple sugars[13, 36,37,38,39,40]. MD simulations have the advantage of not averaging over all equilibrium conformers, but look at a specific structure. In 1996 Liu and Brady[13] conducted MD simulations for 7 different pentopyranoses (β-D-xylopyranose, α-D-xylopyranose, β-D-xylopyranose in $^{1}C_4$, β-D-lyxopyranose, α-D-arabinopyranose, β-L-xylopyranose, α-L-arabinopyranoe. See Figure 6). It was found, as predicted by Galema, that α-L-arabinopyranose, which comprises under group 3 (see Table 1 and Table 2), and is similar to β-D-galactopyranose, indeed made the most hydrogen bonds to water. β-D-lyxopyranose, β-D-xylopyranose and α-D-xylopyranose, which belong to group 2, had more hydrogen bonds than β-D-xylopyranose ($^{1}C_4$), α-D-arabinopyranose and β-L-xylopyranose, which belong to group 1. β-D-xylopyranose ($^{1}C_4$), α-D-arabinopyranose and β-L-xylopyranose all had more favourable internal energies but had unfavourable interaction energies. The favourable internal energy was explained by the possibility to make internal hydrogen bonds between next nearest axial hydroxyl-groups. This would lead to a lower number of hydrogen bonds to the solvent. β-D-xylopyranose ($^{1}C_4$), α-D-arabinopyranose and β-L-xylopyranose were also found to have a higher degree of hydrophobic hydration.

Density mapping of water around α-L-arabinopyranose, β-D-lyxopyranose, β-D-xylopyranose and α-D-xylopyranose revealed tubes of increased (and decreased) density compared to bulk water. This was in contrast to β-D-xylopyranose ($^{1}C_4$), α-D-arabinopyranose and β-L-xylopyranose that had very localised regions with increased water density. It was suggested that the most favourable hydration would occur for those solute molecules whose functional groups are arranged such that their hydration requirements are mutually compatible. β-D-lyxopyranose, β-D-xylopyranose and α-D-xylopyranose and especially α-L-arabinopyranose had favourable hydration and therefore had compatible hydration requirements. This is not in agreement with the modified stereo specific hydration model of Galema where α-L-arabinopyranose will be least compatible to water. It is here reasonable to question what makes a solute compatible to water. Galema argue that a solute has good compatibility to water because of few hydrogen bonds between solute and water, low hydration number and thereof higher apparent hydrophobicity. Liu and Brady argue that

a good compatibility to water arise with increasing hydrogen bonding to solute and favourable solvation energies.

Molteni and Parrinello have conducted a simulation of Glucose in aqueous solution by first principles MD[38]. The idea that the solvation shell of β-glucopyranose should resemble a trydimite ice lattice structure was not supported. This stands in contrast to the results obtained by Sidhu et.al.[41], which tends to confirm the idea of a tridymite ice lattice structure around β-D-glucopyranose.
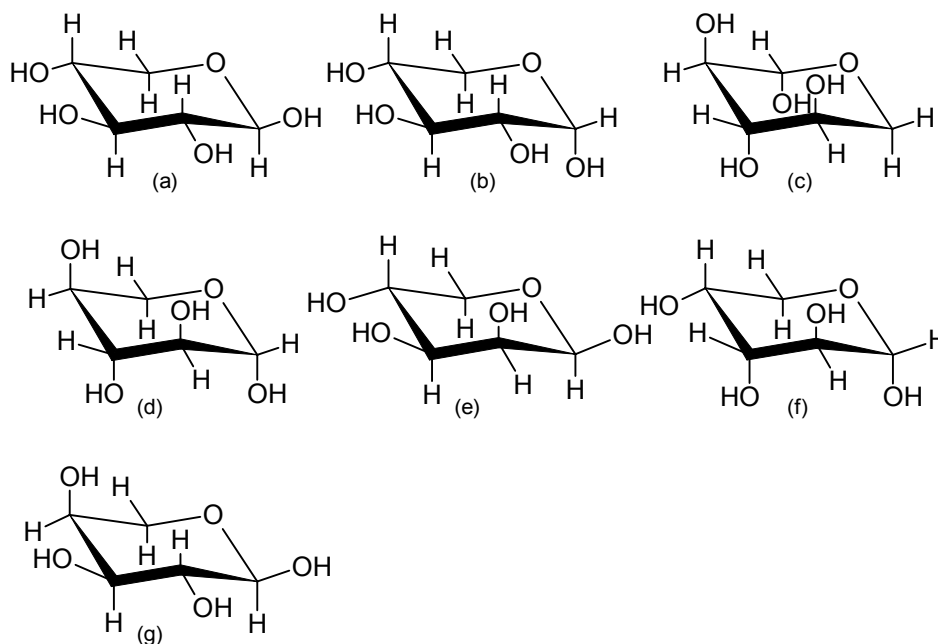
Figure 6   Pentoses modelled by Liu and Brady in ref. 13:   (a) α-D-xylopyranose; (b) β-D-xylopyranose; (c) α-D-xylopyranose in $^{1}C_{4}$ conformation; (d) β-L-xylopyranose; (e) α-D-lyxopyranose; (f) α-D-arbinopyranose; (g) α-L-arabinopyranose

Despite these contrasting views there is general agreement that the hydration of carbohydrates is dependent on the relative positions of hydroxyl-groups and not solely on its fit into a hexagonal water structure similar to ice.

1.4 Approach to the problem

Hydration properties for carbohydrates at atmospheric pressure have been extensively investigated. There is a general agreement that the hydration is very stereo-specific and that the relative positions of hydroxyl-groups are important.

Little is known about hydration at high pressure. At pressures above 1000 bar the anomalous behaviour of water diminish and water behaves more like an ordinary solvent. Owing to this, it is expected that the hydration of carbohydrates will change with increasing pressure.

The easiest way to obtain hydration properties at high pressure is by speed of sound measurements at high pressure. This method has been used before[42,43,44,45] and has been proven to be informative of hydration characteristics of solutes. Using an iterative method one can obtain partial molar volume, partial molar compression, hydration number and all of which are informative of the hydration[34,46]. From these data it is possible to calculate the

8

pressure derivative of partial molar compression and it was desirable to examine whether this physical property would reveal new information to hydration of carbohydrates.

A disadvantage with speed of sound measurements at high pressure is that it does not give direct information about hydration, but give information about effects caused by changes in hydration properties. It is thus influenced by changes in equilibrium caused by complex mutarotation that might occur as pressure increase.

Three aldohexoses: D-glucose, D-galactose and D-mannose, and two aldopentoses: D-ribose and L-arabinose were chosen. These all exist naturally and are thereof biological important. Unfortunately, none of these belong to group 1 in the modified stereo specific hydration model.

2 Thermodynamic properties

The notation of Blandamer is used and previously thermodynamic properties like partial molar compressibility (K_2), coefficient of compressibility (β or κ), partial molar expansibility (E_2) and coefficient of expansibility (α) are here referred to as partial molar compression, compressibility, partial molar expansion and expansivity, respectively.

2.1 Partial molar volume

The partial molar volume of a solute solvated in a solvent is given as

Equation 4
$$V_2 = \left(\frac{\partial V}{\partial n_2} \right)_{T,P,n_1}$$

where V_2 is the partial molar volume, n_2 is moles of substance 2, T is temperature, P is pressure, n_1 is moles of compound 1, i.e. the solvent, and V is the total volume of solution.

Both V_1 and V_2 are Lewisian partial molar properties, as defined by Reis[47] and with the use of Euler's Theorem the total volume is given by

Equation 5
$$V = n_1 V_1 + n_2 V_2$$

This equation can be re-expressed using the molar volume of the pure solvent. Then

Equation 6
$$V = n_1 V_1^* + n_2 V_{\phi,2}$$

where V_1^* is the molar volume of pure n_2 solvent at the same temperature and pressure. Here $V_{\phi,2}$ is the apparent molar volume of solute 2 as defined by Harned and Owen[48]
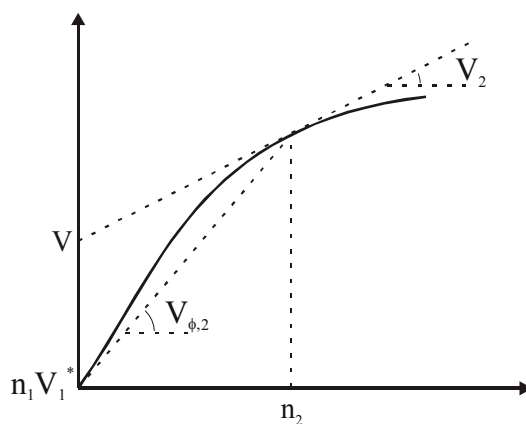
Figure 7   Volume V of a solution as function of the amount of solute 2, n_2, at fixed amount of solvent n_1, temperature and pressure.

10

As shown in figure 1, $V_{\phi,s}$ is the slope of the line joining V at a given amount of compound 2 with fixed amount of solvent[20].

The partial molar volume of compound 2 can now be expressed in terms of the apparent molar volume as given in Equation 7.

Equation 7
$$V_2 = V_{\phi,2} + m\left[\frac{\partial V_{\phi,2}}{\partial m}\right]$$

where m is the molality of the solution in mol solute per kg solvent. From Equation 7 we see that the limiting partial molar volume at infinite dilution equals the limiting apparent molar volume.

Equation 8
$$\lim(m \to 0)V_2 = V_2^\infty = V_{\phi,2}^\infty$$

In order to determine the apparent volume experimentally one measures the density of a solution of a known concentration. Using Equation 6, apparent molar volume as function of density of solvent and solution, molality and molar mass the apparent molar volume is[48]

Equation 9
$$V_{\phi,2} = \frac{\rho^* - \rho}{m\rho\rho^*} + \frac{M_m}{\rho}$$

where ρ is density, M_m molar mass and an asterisk, *, indicates pure solvent.

The apparent partial molar volume cannot be attributed to a physical property of the solution and hence should not be discussed or compared with other solutions. Limiting partial molar volumes are the ones to discuss and compare. The limiting partial molar volume is the difference in volume that is caused by mixing one mole of solute with an infinite volume of solvent so that the solution that becomes is ideal.

2.2 Partial molar expansion

The definition of expansion is

Equation 10
$$E = \left[\frac{\partial V}{\partial T}\right]_P$$

Differentiating Equation 10 with respect to temperature at fixed pressure yield

Equation 11
$$E = n_1 E_1^* + n_2 E_{\phi,2}$$

where E_1^* and $E_{\phi,2}$ are the partial molar expansion of pure solvent and the apparent molar expansion, respectively. Differentiating of Equation 11 with respect to n_2 at fixed n_1, T and P and replacing n_2 with $m \cdot M_m$ (molality times molar mass of solute) yield

Equation 12
$$E_2 = E_{\phi,2} + m\left[\frac{\partial E_{\phi,2}}{\partial m}\right]$$

As for partial molar volume the limiting partial molar expansion equal the limiting apparent molar expansion.

Equation 13
$$\lim(m \to 0)E_2 = E_2^\infty = E_{\phi,2}^\infty$$

Apparent molar expansion can be determined experimentally with

Equation 14
$$E_{\phi,2} = \frac{(\alpha - \alpha^*)}{m\rho^*} + \alpha V_{\phi,2}$$

where α and α^* is the expansivity of solution and pure solvent, respectively, given by

Equation 15
$$\alpha = \frac{1}{V}\left[\frac{\partial V}{\partial T}\right]_p$$

Replacing volume by molecular weight divided by density give

Equation 16
$$\alpha = -\frac{1}{\rho}\left[\frac{\partial \rho}{\partial T}\right]_p$$

2.2.1 Calculation of expansivity

Ideally one could fit density trough linear regression and use the definition given in Equation 15 and Equation 16 to calculate α for each concentration. A problem is that this method is inflicted with a relatively large error due to few measure points. A better way is to fit the difference between density of the solution and water and use this equation to calculate α.

Equation 17
$$\rho - \rho^* = a_0 + a_1 T + a_2 T^2$$

Equation 18
$$\left(\frac{\partial(\rho - \rho^*)}{\partial T}\right) = a_1 + 2a_2 T$$

The left side of Equation 18 can be reorganised to

Equation 19
$$\left(\frac{\partial \rho}{\partial T}\right) - \left(\frac{\partial \rho^*}{\partial T}\right) = -\alpha \cdot \rho + \alpha^* \rho^*$$

The expression for α then becomes

Equation 20
$$\alpha = -\frac{a_1 + 2a_2 T}{\rho} + \frac{\alpha^* \rho^*}{\rho}$$

2.3 Partial isothermal molar compression

The isothermal compression is given by

Equation 21
$$K_T = -\left[\frac{\partial V}{\partial p}\right]_T$$

The term compression is used instead of compressibility as recommended by Blandamer[20]. Differentiating Equation 21 with respect to pressure at fixed temperature yield

Equation 22
$$K_T = n_1 K_{T,1}^* + n_2 K_{T,\phi,2}$$

where, by definition, the apparent molar isothermal compression of solute 2, $K_{T,\phi,2}$ and partial molar compression of pure solvent, $K_{T,1}^*$, is given by

Equation 23
$$K_{T,\phi,2} = -\left[\frac{\partial V_{\phi,s}}{\partial p}\right]_T$$

Equation 24
$$K_{T,1}^* = -\left[\frac{\partial V_1^*}{\partial p}\right]_T$$

Differentiation of Equation 22 with respect to n_2 at fixed n_1, T and p, and replacing n_2 with $m \cdot M_m$ (molality times molar mass) yield

Equation 25
$$K_{T,2} = K_{T,\phi,2} + m\left[\frac{\partial K_{T,\phi,2}}{\partial m}\right]$$

As for partial molar volume, the limiting partial isothermal compression at infinite dilution equals the limiting apparent molar compression.

Equation 26 $$\lim(m \to 0)K_{T,2} = K_{T,2}^{\infty} = K_{T,\phi,2}^{\infty}$$

$K_{T,\phi,2}$ can be determined experimentally by

Equation 27 $$K_{T,\phi,2} = \frac{\kappa_{T,2} - \kappa_T^*}{m\rho^*} + \kappa_{T,2}V_{\phi,2}$$

where κ_T is the isothermal compressibility given by

Equation 28 $$\kappa_T = -\frac{1}{V}\left[\frac{\partial V}{\partial p}\right]_T = \frac{1}{\rho}\left[\frac{\partial \rho}{\partial p}\right]_T$$

2.4 Partial isentropic molar compression

It is difficult to determine $\kappa_{T,2}$ experimentally. A more convenient path is to use the Newton-La Place equation[49] to get the isentropic compressibility from speed of sound and density data given in Equation 29 where u is speed of sound in cm/s and ρ is density in g/cm³.

Equation 29 $$\kappa_S = \frac{100}{u^2\rho}$$

The relation between isothermal and isentropic compressibility is given by

Equation 30 $$\kappa_T = \kappa_S + \frac{\alpha^2 T}{\sigma_p}$$

where α is the expansivity defined in Equation 15 and σ_p is the isobaric heat capacity for unit volume of solution defined as

Equation 31 $$\sigma_p = \frac{C_p}{V}$$

Now one might think that there would be an equal expression for the apparent isentropic molar compression as there is for the apparent isothermal compression in Equation 27. But the entropy is not constant as concentration varies, and specifically the entropy of pure solvent and solution is not the same[21]. Harned and Owen[48] used the symbol "equivalent to",≡, when defining $K_{S,\phi,2}$. Blandamer defined it, as a practical apparent isentropic compression, which he showed, is not a thermodynamically correct variable[20].

Equation 32
$$K_{S,\phi,2,\text{prac.}} \equiv \frac{\kappa_S - \kappa_S^*}{m\rho^*} + V_{\phi,2}\kappa_S$$

The thermodynamically correct apparent molar isentropic compression is

Equation 33
$$K_{S,\phi,2} = \frac{\kappa_S - \kappa_S^*}{m\rho^*} + V_{\phi,2}\kappa_S + \frac{1}{m\rho^*} \times T\alpha^* \left\{ \frac{\alpha}{\sigma} - \frac{\alpha^*}{\sigma^*} \right\}$$

Most works reporting apparent isentropic compression use Equation 32. For convenience and comparison Equation 32 is also used in this work, but recognised as practical apparent isentropic compression.

One should be careful to discuss limiting partial isentropic compression, derived either from apparent or practical apparent isentropic molar compression, from the fact that the entropy of pure solvent and solution are different[20,21].

2.5 Apparent molar compression as function of pressure

In order to calculate the apparent molar isothermal compression at applied pressure the density of pure solvent and solution is needed (Equation 27 and Equation 28). The density of water at elevated pressure is taken from "The equation of state of pure water determined from sound speeds" of Chen, Fine and Millero[50]. The density of the solution is more difficult to obtain. It was estimated using an iterative process based on the speed of sound data first outlined by Vikingstad et.al.[43]. Maldal[44] changed the starting point and this is the one used in this work with the introduction of the adiabatic constant, γ, and use of apparent isothermal molar compression instead of apparent isentropic molar compression.

2.5.1 An iterative method for an estimate of density and compression at elevated pressure

The first step is to estimate density. Equation 28 and Equation 29 give the relation between the speed of sound data and the density.

Equation 34
$$\left(\frac{\partial \rho}{\partial p} \right)_S = \frac{100}{u^2}$$

An integrated power series from the speed of sound data at elevated would give density as function of pressure. However, there is reason to question constant entropy as pressure increases. To circumvent this an adiabatic-constant, γ, is introduced to give isothermal compressibility from isentropic compressibility.

Equation 35
$$\gamma = \frac{\kappa_T}{\kappa_S} = \frac{\kappa_S + \dfrac{\alpha^2 T}{\sigma_p}}{\kappa_S} = 1 + \frac{\alpha^2 T}{\sigma_p \kappa_S}$$

An assumption is made in that $\dfrac{d\gamma}{dp}$ is assumed to be equal to $\dfrac{d\gamma^*}{dp}$. Hence

Equation 36
$$\gamma(p) = \gamma(0) - \gamma^*(0) + \gamma^*(p)$$

The equation of state of pure water by Chen, Fine and Millero[50] can be used to give γ^* as function of pressure.

Equation 37
$$\left(\frac{\partial \rho}{\partial p}\right)_T = \frac{100\gamma(p)}{u(p)^2} = a_0 + a_1 p + a_2 p^2 + a_3 p^3$$

Density as function of pressure can then be found by integrating Equation 37

Equation 38
$$\rho(p) = \int_{p=0}^{p} \left(a_0 + a_1 p + a_2 p^2 + a_3 p^3\right) dp = \rho(0) + a_0 p + \frac{1}{2}a_1 p^2 + \frac{1}{3}a_2 p^3 + \frac{1}{4}a_3 p^4$$

Equation 38 and Equation 37 is the starting point of the iterative method. Using Equation 38 the apparent molar volume, the isothermal compressibility and then from Equation 27 the apparent molar isothermal compression can be calculated at each measured pressure.

An integrated power series from the apparent molar isothermal compression at measured pressures gives new values for the apparent molar volume at each measured pressure.

Equation 39
$$K_{T,\phi,2} = -\left[\frac{\partial V_{\phi,2}}{\partial p}\right]_T = b_0 + b_1 p + b_2 p^2 + b_3 p^3$$

Equation 40
$$V_{\phi,2} = V_{\phi,2}(0) + b_0 p + \frac{1}{2}b_1 p^2 + \frac{1}{3}b_2 p^3 + \frac{1}{4}b_3 p^4$$

Equation 41
$$\rho = \frac{\left(1 + m \cdot M_m\right)}{\left(m \cdot V_{\phi,2} + \dfrac{1}{\rho^*}\right)}$$

Densities are calculated from the new $V_{\phi,2}$ data and the process starts over again. It stops when

Equation 42
$$\left| \frac{K_{T,\phi,2,n+1}}{K_{T,\phi,2,n}} \right| - 1 < 0,001$$

where $K_{T,\phi,2,n+1}$ is the n+1th iteration and $K_{T,\phi,2,n}$ is the nth iteration. Usually n is less than 4.

2.5.2 An alternative method

Including temperature as an variable in addition to pressure, speed of sound and concentration would make it possible to calculate all P-V-T properties with the use of the method first described by Lance A. Davis and Robert B. Gordon[45,51,52]. This method is more accurate and is not depending on the assumption that $\frac{d\gamma}{dp}$ is equal to $\frac{d\gamma^*}{dp}$.

2.6 Hydration number

Hydration number is an informative measure for the hydration layer. Different definitions and techniques exist. Using NMR and dielectric studies, Tait et.al.[26] defined the hydration number as the average number of water molecules hydrogen bonded to the solute so that the bond lasts longer than in water. Galema and Høiland[22] obtained hydration number from speed of sound and density measurements and defined it as an indication to the number of water molecules disturbed by the presence of a solute molecule. Common for all hydration numbers is that a large hydration number indicates a large deviation in water structure of the hydration shell from the water structure in the bulk. The absolute value of hydration number depends on the method used[53], but the relative trends are the same.

Hydration number, n_H can be obtained from speed of sound experiments trough a method described earlier[45,53,54].

Equation 43
$$n_H = \frac{n_w}{n_s} \left(1 - \frac{\kappa_S}{\kappa_S^*} \right)$$

where n_w and n_s are the mole fractions of water and carbohydrate, respectively. Equation 43 assumes that the compressibility of the hydration layer is zero. This affects the hydration number, but leaving the trend in the numbers unchanged[41].
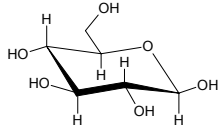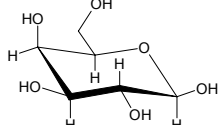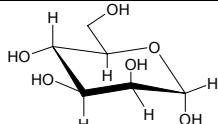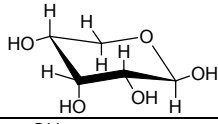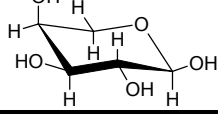
2.7 Pressure derivative of partial isothermal molar compression

Given that $K_{T,2}$ can be obtained as a function of pressure, one can calculate the pressure derivative, $\left[\frac{\partial K_{T,2}^{\infty}}{\partial p} \right]$. This property can give information about concavity of $K_{T,2}$ as function of pressure.

3 Experimental

3.1 Chemicals

Table 3   Specifications of chemicals used.

Sugar	Purity	Anomer comp.	dominant conformer[a]	M_m, $g \cdot mol^{-1}$	Manufacturer
D(+) glucose	N/A, anhydrous	Specific rot: 52,8° at 25 °C		180,156	Sigma
D(+) galactose	min 99%	N/A		180,156	Sigma
D(+) mannose	min 99%	6% β, 94% α		180,156	Sigma
D(-) ribose	min 99,0%	N/A		150,12	Sigma
L(+) arabinose	min 99%	N/A		150,12	Sigma

[a] See Table 1 page 3

All carbohydrates were dried for 24 hours in a vacuum exicator. Solutions were prepared with distilled water and made in the molality scale with Mettler PE 3600 weight with an accuracy of 0,01g and a Mettler AE 163 weight with an accuracy of 0,0002g. All solutions were allowed at least two hours to stabilise. Due to bacterial degradation it was crucially important that all measurements were performed within a week and that the solutions were stored in a refrigerator. The same solutions were used for the density and speed of sound measurements.

3.2 High pressure equipment

The pressure piping was constructed using existing and new parts. Its maximum pressure tolerance is 2000 bar. Table 4 lists specifications of each part. See A.II page 45 for operation manual.

Table 4   Specifications of high-pressure equipment parts

Part	Producer	Type, material	Max. pressure
Tubing	Autoclave Engineers	MS15-081, 316 ss	60 000 psi
Fittings/Valve B	Pressure Products	316 ss	60 000 psi
Hand pump	Enerpac	P-228	40 000 psi
Manometer	Budenberg		3000 bar
Pressure sensor	Hottinger Baldwin Messtechnik, HBM	P 3 M	2000 kp/cm^2
Pressure vessel	Christian Michelsen Institutt on commission for UiB	steel	>2 000 bar
Hydraulic oil	Hydro/Texaco	Rando hdz 15	very high
Timer	Phillips	6666	not pressure equipment

3.2.1 Calibration of pressure sensor

A dead-weight pressure gauge tester from Dreyer, Rosenkrantz + Droop A.G. was used to calibrate the pressure sensor. An Oltronix Power Supply B3000 gave a voltage of 10,000±0,001 V. A HP 3465 Digital multimeter measured the voltage across the pressure sensor. The data was fitted to a polynomial function of 2nd degree to give applied pressure; that is, absolute pressure minus atmospheric pressure. See Table 21. The error was estimated with a 95% confidence interval to be less than ±0.3 bar for all pressures in the range of 200 to 2000 bars.

3.2.2 Temperature control

The pressure vessel was placed in an isolated steel cylinder with a volume of approx. 60 L, filled with hydraulic oil. Temperature of the oil and the pressure vessel were controlled with a Heto Birkerød temperature controller. The oil was cooled with water from a water bath thermostated at 13 °C with a Birkerød temperature controller and a Hetofrig cooler. The temperature was measured with a HP 2804 Quartz thermometer with a resolution of 0,001°C. The uncertainty in temperature of the oil was better than ±0,015°C.

3.3 Speed of sound measurements

3.3.1 Principle

The sound velocity can be measured using the sing-around principle[55]. A spike generator generates an electrical pulse. A transducer transforms this electrical pulse into a pressure (sound) pulse. The sound pulse propagates through the solution. A transducer transforms the sound pulse into an electrical pulse. This pulse is amplified and then sent to the spike generator where a new pulse is made. The time of one cycle, averaged over 1second, is measured. This is the time the pressure pulse use to propagate through the solution, t, plus the time the electrical pulse use in the circuit plus an electronic time-delay added in the generator to prevent interference from echoes.

Equation 44 $$t = t_m + \tau$$

where t_m is the measured time and τ is the sum of the electronic time-delay and the time the electrical pulse uses in the circuit.

Given the distance the pressure pulse travel is s, the speed of sound in the solution can be found by

Equation 45
$$u = \frac{s}{t - \tau}$$

where u is the speed of sound, t is time of one cycle and τ is electronic delay.

By measuring the time sound use through a solution with known velocity, in this case pure water, the distance s, i.e. the length of the cell, can be determined. The full expression then becomes

Equation 46
$$u = \frac{u^* \cdot (t^* - \tau)}{t - \tau}$$

where an asterisk indicates pure solvent.

3.3.2 Apparatus

A Philips PM 6666 programmable timer/counter was used to measure the time. The timer was set to average over 1 second. A Telequipment Oscilloscope was used to view and check the signal. All of the ultrasonic equipment are developed and made at the University of Bergen. The ultrasonic frequency is 10 MHz.

Instead of two transducers in the cell a reflector reflect the sound pulse back to the emitting transducer which transform it to an electrical pulse. In order for this to work, the receiver must cut of the original electrical pulse so that only the signal of the reflected sound pulse reach the timer and generates a new pulse.
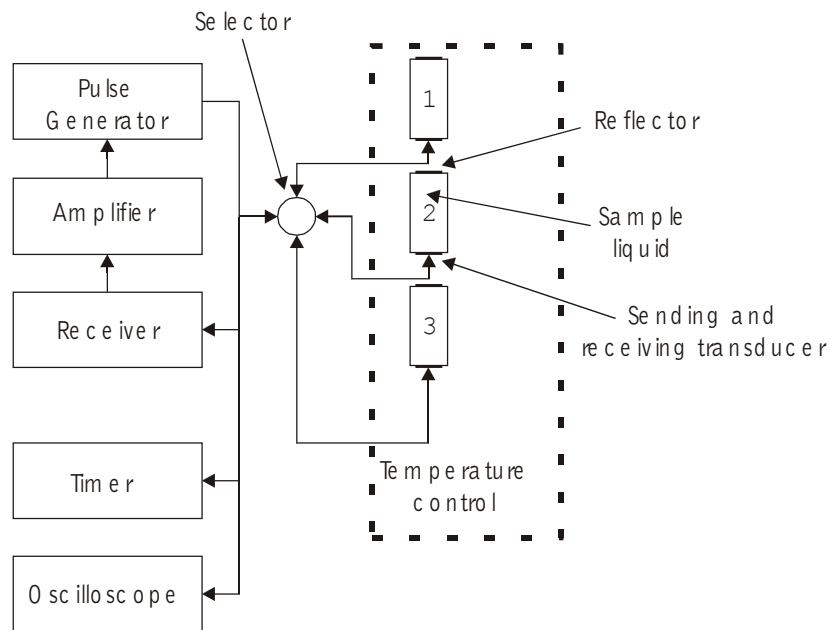
Figure 8   Instrument coupling

Chief Engineer Einar Høgseth and Principal Engineer Steinar Vatne constructed the ultrasonic pressure cells.
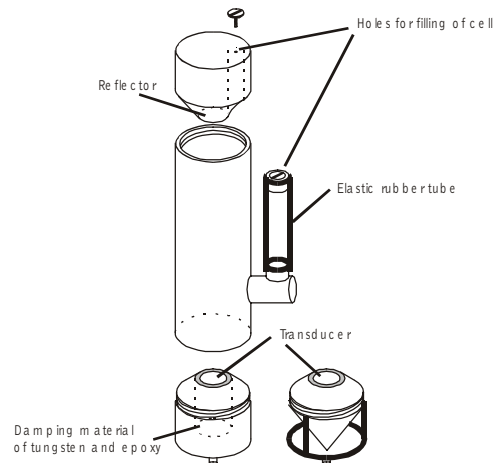
Figure 9   Ultrasonic cell

τ can be measured by comparing measured time obtained by the pulse echo method[56] and sing around method using one cell. The advantage of pulse echo is that it measures the time between two echoes instead of the time used trough the whole circuit with the embedded electronic time-delay. The pulse-echo-time is therefore the true time a sound-pulse needs trough a solution in a cell with length s. In order to use the pulse echo method, a cell with better control of back-reflections had to be used.

Equation 47 $$\tau = t_{sing-araound} - t_{pulse-echo}$$

3.3.3 Application and error

See operation manual in A.II.1 at page 45 for use of ultrasonic equipment.

Due to temperature fluctuation of the oil in the steel cylinder and a long for time, 50 to 90 min., to obtain thermal equilibrium inside the pressure vessel it is difficult to assert an uncertainty to t_m. t_m was noted when the drift in t_m was less than 1 second/second. The error in the calculated speed of sound, u, was obtained by comparison with a reference cell filled with distilled water.

3.3.4 Error in speed of sound measurements

This method has been tested by measuring the difference in velocity of pure water in each cell. The difference at each pressure should be zero, but due to different length, s, temperature fluctuations and compression there are small but noticeable deviations. The accuracy of the velocity measurements was on basis of these measurements estimated to be in the range of $\pm0,04$ till $\pm0,07$ m/s depending on the cell used.

As pressure increased, the path, s, decreased. This decreased the measured time and gave a larger speed of sound value than the true value. A reference cell filled with water was used to reduce this systematic error till negligible. Under the assumption that the reduction in s is equal for each cell the true velocity of the measured solution can be expressed as

Equation 48
$$u(p) = u_m(p) \cdot \frac{u^*(p)}{u_m^*(p)}$$

where p is the given pressure, u_m is the measured velocity of the solution, u_m^* is the measured velocity of water and u^* is the true velocity of water at the given applied pressure. Reference data for u^* at atmospheric pressure were taken from Del Grosso and Mader[57] and at applied pressure from the work of Wilson[58], later corrected by Chen and Millero[59].

Applying Equation 48 also decrease the inaccuracy of measured speed of sound at atmospheric due to the strong dependence of speed sound on temperature[45]. A requirement is that both cells have the same temperature.

3.4 Density measurements

3.4.1 Principle

The density was measured using a density meter connected to a hollow oscillating tube-measuring cell. The frequency of the measure cell is a function of the density of the fluid in the hollow tube. The density meter measures the time for a pre set number of cycles. When the density, d^*, of the solvent is known the density of the solution is given by

Equation 49
$$d - d^* = \frac{1}{A}\left(T^2 - T^{*2}\right)$$

where an asterisk, *, indicates pure solvent, T is time and A is the apparatus constant.

3.4.2 The apparatus constant

A can be found by measuring T for two fluids with known density. It is convenient to use water and air to determine A. The density of air as function of temperature, pressure and relative air humidity is given by Equation 50

Equation 50
$$d_{air} = \left(1{,}2929 \cdot 10^{-3}\right)\left(\frac{273{,}15}{T}\right)\left(\frac{B - 0{,}3783 \cdot e \cdot \frac{F}{100}}{760}\right)$$

where T is room temperature given in Kelvin, B is air pressure given in Torr, F is relative air humidity, and e is vapour pressure of water at the measured temperature. e was estimated at the given room temperature from a second order linear regression of reference data[60]. The densities of water at a given temperature at atmospheric pressure were taken from the work of Kell[61]. The apparatus constant depend on room temperature and therefore must be measured for each measure series.

3.4.3 Apparatus

An Anton Paar K.G. DMA 60 density meter and a DMA 602 density-measuring cell were used. The measure cell was connected to a water bath thermostated by a Heto Birkerød

temperature controller and the temperature in this bath was measured with a Fluke 2180A digital thermometer with a resolution of 0,001°C. The uncertainty in water temperature was lower than 0,003 °C.

3.4.4 Application

The density was measured by carefully injecting the solution into the hollow U-tube with a sterile syringe. The tube holds approximately 1 ml. About 3 ml was injected to the tube so that the tube was flushed with solution. The syringe was held in position and the other end of the tube was gently closed with a rubber plug. After approx. 5 min when temperature was constant the time period was noted. T for both water and air were noted before and after each measure series.

4 Results and discussion

This chapter is divided into four parts. The first part discusses error and uncertainties in raw data and presented data. The second present and discuss results obtained at atmospheric pressure and compare these with some of the existing literature data. The third part presents each limiting property, which are discussed in terms of deviations and general trends. The fourth and final part discusses all properties and interpretation of these.

4.1 Errors

The accumulation of error in Y, which is a function of $X_1, X_2, X_3\ldots$, is given by

Equation 51
$$\Delta Y = \sqrt{\left(\frac{\partial Y}{\partial X_1}\Delta X_1\right)^2 + \left(\frac{\partial Y}{\partial X_2}\Delta X_{21}\right)^2 + \left(\frac{\partial Y}{\partial X_3}\Delta X_3\right)^2 + \ldots}$$

where ΔY is the error in Y and ΔX_1, ΔX_2, $\Delta X_3,\ldots$ is the error in X_1, X_2, $X_3,\ldots$, respectively. Equation 51 is used where appropriate.

4.1.1 Error in calculated properties at atmospheric pressure

Error in concentration were determined by

Equation 52
$$\Delta m = m \cdot \sqrt{\left(\frac{\Delta m_m}{m_m}\right)^2 + \left(\frac{\Delta M_m}{M_m}\right)^2 + \left(\frac{\Delta m_{Solvent}}{m_{solvent}}\right)^2}$$

where m is concentration, m_m is mass of solute, M_m is molar mass of solute and $m_{solvent}$ is mass of solvent.

Error in density was calculated with Equation 51 from Equation 49. The calculated uncertainty was less than $4\cdot10^{-6}\,\text{g}\cdot\text{cm}^{-3}$ for all concentrations.

Equation 53 to Equation 56 give the error of calculated thermodynamic properties.

Equation 53
$$\Delta V_{\phi,2} = \sqrt{\left(\frac{\frac{1000}{m_m}+M_m}{\rho^2}\Delta\rho\right)^2 + \left(\frac{1000\left(\rho^*-\rho\right)}{m^2\rho\rho^*}\Delta m\right)^2 + \left(\frac{1000}{m\rho^{*2}}\Delta\rho^*\right)^2}$$

Equation 54
$$\Delta\kappa_S = \frac{2\cdot100}{u^3\rho}\Delta u$$

The error in density is left out due to insignificant contribution

Equation 55
$$\Delta K_{S,\phi,2,prac} = \sqrt{\left(\left(\frac{1000}{m\rho^*}+V_{\phi,2}\right)\Delta\kappa_S\right)^2 + \left(\kappa_S \Delta V_{\phi,2}\right)^2}$$

The error in concentration and density of solvent are left out due to insignificant contribution.

Equation 56
$$\Delta\kappa_T = \sqrt{\Delta\kappa_S{}^2 + \left(\frac{2\alpha T}{\sigma_p}\Delta\alpha\right)^2 + \left(\frac{\alpha^2 T}{\sigma_p{}^2}\Delta\sigma_p\right)^2}$$

The equation for $\Delta K_{T,\phi,2}$ is similar to Equation 55.

Table 5   Errors that are constant or determined to be less than the given value.

	ρ	α	u	σ_p	γ
Error	$4\cdot10^6$ g·cm^{-3}	$0,5\cdot10^6$ K^{-1}	0,04-0,07 m·s^{-1}	0,01 bar·K^{-1}	$5\cdot10^{-5}$

Table 6   Uncertainties in reported data for D-galactose at atmospheric pressure and 25 °C

concentration, molal	concentration, molal	$V_{\phi,2}$	$K_{S,\phi,,2,\,prac.}$	$K_{S,\phi,2}$
0,06346	0,00003	0,07	0,38	0,48
0,10279	0,00003	0,04	0,23	0,30
0,11873	0,00002	0,04	0,20	0,26
0,15094	0,00003	0,03	0,16	0,20

Both $K_{S,\phi,,2,\,prac.}$ and $K_{S,\phi,2}$ were calculated at atmospheric pressure. The relative difference was less than 0,02% for all sugars and concentration. The low differences are related to low concentrations, but also reflect the favourable hydration of the studied sugars.

The difference in error between $K_{S,\phi,,2,\,prac.}$ and $K_{T,\phi,2}$ is very small. The error in $K_{T,\phi,2}$ in large stem from the error in measured speed of sound, and not α or σ_p.

4.1.2 Ultrasonic equipment

As mentioned above in 3.3.4 on page 21, it was not possible to measure the absolute speed of sound without the use of a reference cell and reference data. There are several possible systematic errors that would cause a deviation in the speed of sound data.

Apparent molar volume, $V_{\phi,2}$, and apparent molar compression, $K_{X,\phi,2,}$ were both calculated assuming that cell length, s, was constant or that the measured pressure was correct. Assuming that the cell length, s, was constant the true pressure was calculated from the measured speed of sound in water. Results for $V_{\phi,2}$ and $K_{X,\phi,2}$ using the described methods are given in Table 8 and Table 9. Table 10 list estimated $V_{\phi,2}$ and $K_{X,\phi,2}$ for both methods at equal pressures. Both methods give almost equal results for $V_{\phi,2}$ at all pressure. There is a small deviation in $K_{X,\phi,2}$ at pressures below 600 bar. It is believed that this in large stem from a difference in temperature between calibration and measurement and hence a difference in measured speed of sound. Assuming that the measured pressure was correct and using Equation 48 at page 22 gave a better correlation to previously measured speed of sound data[62,63,17] at atmospheric pressure and this method is the one used.

Table 7   Systematic errors

Part	Problem	Effect on cell lenght,s.
Rubber hose	Lower pressure inside the cell	Apparent longer cell
Transducer	Pressed into the back	Longer cell
Ultrasonic cell body	Deformation	Most likely shorter
Pressure sensor	Is placed outside the pressure vessel where there is a lower temperature	Apparent shorter cell
Transducer	Swelling	Shorter cell
Ultrasonic cell	No stirrer mixed the solution so that equilibrium took long time to be obtained.	
All other parts	Electrical distortion	Unknown
Calibration of s	Difference in temperature between calibration and measurement of solution	Both

Table 8 $V_{\phi,2}$ and $K_{T,\phi,2}$ calculated with the assumption of correct measured pressure. Data is for $0{,}15094 \pm 0{,}00003$ molal D-galactose.

	Start of iteration		Final result of iteration	
Applied pressure, bar	$V_{\phi,2}$, $cm^3 mol^{-1}$	$K_{T,\phi,2}$, $10^6 cm^3 mol^{-1} bar^{-1}$	$V_{\phi,2}$, $cm^3 mol^{-1}$	$K_{T,\phi,2}$, $10^6 cm^3 mol^{-1} bar^{-1}$
0,0	110,44	-16,37	110,44	-16,37
199,3	110,71	-13,77	110,74	-13,75
405,1	110,97	-11,32	110,99	-11,30
602,9	111,17	-9,09	111,19	-9,08
800,1	111,33	-6,89	111,35	-6,88
1007,1	111,45	-5,06	111,47	-5,05
1203,4	111,54	-3,35	111,56	-3,34
1400,1	111,59	-1,95	111,61	-1,93

A problem when using water as a reference is that there does not exist accurate speed of sound in water data at pressures above 1000 bar. Smith and Lawson[64] report data in the range 261 – 402 K and 1-9230 bar, and Litowitz and Carnevale[65] report data at 273 and 303 K at pressures ranging from 1-196 bar, but these are not accurate enough for this work to be compared with the re-evaluated data of Wilson and hence cannot be used[66]. Hillbert[67] report density data at 293-873 K at pressures ranging from 10-400 MPa. Using the equation of state[50] calculated from the re-evaluated speed of sound data of Wilson[58,59] one can estimate the extrapolated density at a given measure point of Hillbert. The extrapolated density falls within the reported limit of uncertainty. The extrapolated speed of sound and density data is therefore assumed to be accurate. The data of Hillbert cannot be used to estimate density at 25°C due to few data points. All data of comparing references were taken from the review article of Sato et.al[66].

The cells with a back-absorber of epoxy mixed with tungsten gave the best reproducibility, but were notoriously unstable at high pressures probably due to compression of the transducer. These cells were also very old, and had to be discarded after some use. A new cell design was made, which had a coned brass back-absorber (see Figure 9 at page 21). They were more stable, but had a larger uncertainty. The higher uncertainty made it more difficult to estimate the apparent molar compression, $K_{T,\phi,2}$, due to the small difference in compressibility of water, κ_T^*, and solution, κ_T.

The electronic time delay, measured with the method described in 3.3.2 page 20, was found to be 1,62±0,01 μs.

Table 9 $V_{\phi,2}$ and $K_{T,\phi,2}$ calculated with the assumption of constant cell length pressure. Data is for 0,15094±0,00003 molal D-galactose.

Applied pressure, bar	Start of iteration		Final result of iteration	
	$V_{\phi,2}$, cm^3mol^{-1}	$K_{T,\phi,2}$, $10^6cm^3mol^{-1}bar^{-1}$	$V_{\phi,2}$, cm^3mol^{-1}	$K_{T,\phi,2}$, $10^6cm^3mol^{-1}bar^{-1}$
0,0	110,44	-16,30	110,44	-16,30
199,6	110,71	-13,70	110,73	-13,68
407,1	110,97	-11,25	110,99	-11,23
606,9	111,17	-9,01	111,19	-9,00
806,6	111,33	-6,81	111,35	-6,79
1016,6	111,46	-4,97	111,47	-4,96
1215,0	111,54	-3,26	111,56	-3,25
1414,3	111,59	-1,86	111,61	-1,85

[a] Correct pressures are calculated from measured speed of sound data with the use of ref.59.

Table 10   Comparison of $V_{\phi,2}$ and $K_{T,\phi,2}$ with the assumption of correct measured pressure or constant cell length. Data is for 0,15094±0,00002 molal D-galactose.

Applied pressure, bar	Correct measured pressure		Constant cell length[a]	
	$V_{\phi,2}$, cm^3mol^{-1}	$K_{T,\phi,2}$, $10^6cm^3mol^{-1}bar^{-1}$	$V_{\phi,2}$, cm^3mol^{-1}	$K_{T,\phi,2}$, $10^6cm^3mol^{-1}bar^{-1}$
0	110,44	-16,37	110,44	-16,30
200	110,74	-13,78	110,74	-13,72
400	110,99	-11,34	110,99	-11,29
600	111,19	-9,06	111,19	-9,02
800	111,35	-6,96	111,35	-6,94
1000	111,47	-5,06	111,47	-5,05
1200	111,56	-3,38	111,55	-3,38
1400	111,61	-1,93	111,60	-1,94

[a] Correct pressures are calculated from measured speed of sound data with the use of ref. 59.

4.1.3 The iterative process

The iterative process previously used[43] did not include the adiabatic constant, γ, in Equation 37. and apparent isothermal molar compression, $K_{T,\phi,2}$, in Equation 39. Instead isentropic compression and compressibility were used. Applying isentropic variables in the iterative process one has to assume that the entropy is constant as pressure varies.

With the density data from Helland[62] and heat capacities from Galema et.al[34] the isothermal compressibility and γ could be calculated at atmospheric pressure (See Equation 35 page 16). Table 11 and Table 12 list $V_{\phi,2}$ and $K_{X,\phi,2}$ at the start of the iteration, calculated with Equation 38, and the final result.

By using γ at the start of the iteration there is no significant change in neither $V_{\phi,2}$ or $K_{X,\phi,2}$. This clearly shows that the assumption made in 2.5.1 page 15 that change in γ as pressure varies is equal to the change in γ^*, is legitimate. For lower concentrate solutions there is a significant change in $V_{\phi,2}$ from start of iteration to final result. This change is less than 0,1%

for all pressures and is a result of the small difference in speed of sound between pure solvent and solution.

It is believed that the uncertainties at elevated pressures are less than 20% higher than the calculated uncertainty at atmospheric pressure.

Table 11   Iterative process without the use of γ exemplified with 0,15094±0,00003 molal D-galactose. Uncertainties at atmospheric pressure are given in parenthesis.

Applied pressure, bar	Start of iteration		Last iteration	
	$V_{\phi,2}$, cm^{3}mol^{-1}	$K_{S,\phi,2,\,prac}$, 10^6cm^{3}mol^{-1}bar^{-1}	$V_{\phi,2}$, cm^{3}mol^{-1}	$K_{S,\phi,2,\,prac}$, 10^6cm^{3}mol^{-1}bar^{-1}
0,0	110,44	-19,95	110,44	-19,95
	(0,03)	(0,16)	(0,04)	(0,16)
199,3	111,46	-16,49	110,80	-17,03
405,1	112,57	-13,18	111,13	-14,32
602,9	113,69	-10,15	111,38	-11,87
800,1	114,83	-7,17	111,60	-9,49
1007,1	116,08	-4,55	111,77	-7,48
1203,4	117,28	-2,13	111,90	-5,64
1400,1	118,50	-0,06	111,99	-4,12

Table 12   Iterative process with the use of γ exemplified with 0,15094±0,00003 molal D-galactose. Uncertainties at atmospheric pressure are given in parenthesis.

Applied pressure, bar	Start iteration		Last iteration	
	$V_{\phi,2}$, cm^{3}mol^{-1}	$K_{T,\phi,2}$, 10^6cm^{3}mol^{-1}bar^{-1}	$V_{\phi,2}$, cm^{3}mol^{-1}	$K_{T,\phi,2}$, 10^6cm^{3}mol^{-1}bar^{-1}
0,0	110,44	-16,37	110,44	-16,37
	(0,03)	(0,24)	(0,03)	(0,24)
199,3	110,71	-13,77	110,74	-13,75
405,1	110,97	-11,32	110,99	-11,30
602,9	111,17	-9,09	111,19	-9,08
800,1	111,33	-6,89	111,35	-6,88
1007,1	111,45	-5,06	111,47	-5,05
1203,4	111,54	-3,35	111,56	-3,34
1400,1	111,59	-1,95	111,61	-1,93

4.1.4 Limiting properties

Given a function $y = a_0 + a_1 x$ that is obtained trough first order linear regression. The confidence interval for the true a_0, $\hat{a}_0$, is given by

Equation 57
$$\hat{a}_0 = a_0 \pm \frac{t_{\alpha/2} s \sqrt{\sum x_i^2}}{\sqrt{n \sum (x_i - \bar{x})^2}}$$

where $t_{\alpha/2}$ is the student's t value at a (1-α) 100% confidence level with n-2 degrees of freedom, s is the standard deviation of a_0, n is the sample size, x_i is sample i, and $\bar{x}$ is the mean of all x.

Equation 57 can be rewritten to

Equation 58 $$\hat{a} = a_0 \pm t_{\alpha/2} S_{a_0}$$

where S_{a_0} is the standard error often given in regression software.

Measuring speed of sound as function of pressure for a given concentration took 1 day plus measure series that had to be discontinued. It was therefore not possible to measure more than 4 concentrations for each sugar (only 3 for L-arabinose). Calculating limiting properties with only 4 concentrations give a wide confidence interval due to few degrees of freedom. Another problem is that some of the properties display only small concentration dependence. All errors in limiting properties at atmospheric pressure are calculated with the use of Equation 58, except those of L-arabinose, which became very high. Errors in L-arabinose are obtained with a qualified guess bearing in mind the inherent uncertainty, scatter and comparison with other sugars.

Equation 58 does not include the inherent error of each data point. For some properties, like V_2^∞ for D-glalactose, there is a very low standard error that give a confidence interval lower than the error in each point. In such cases error in V_2^∞, $K_{X,2}^\infty$ and n_H are all set higher than 0,7 $cm^3 mol^{-1}$, $0,7 \cdot 10^6 cm^3 mol^{-1} bar^{-1}$ and 0,1 , respectively. The larger error (20%) in $K_{T,\phi,2}$ compared to $K_{S,\phi, prac.,2}$ does not contribute to a larger error in $K_{T,2}^\infty$. Error in $K_{T,2}^\infty$ stem from linear regression.

4.2 Atmospheric pressure

There are extensive data for the investigated monosaccharides at atmospheric pressure. Table 13 and Table 14 list data from this work and literature values. Figure 10 and Figure 11 show concentration dependence of $V_{\phi,2}$.

Table 13   Limiting properties for the aldoses D-glucose, D-galactose and D-mannose at atmospheric pressure. Literature values are given in parenthesis.

	D-glucose	D-galactose	D-mannose
V_2^{∞}, cm^3/mol	111,97±0,10 (111,91±0,09)[a] (112,2±0,4)[c] (111,9)[d] (111,7±0,3)[e] (112,0±0,1)[h]	110,31±0,07 (110,29±0,04)[a] (111,9±0,3)[c] (110,7)[d] (110,2±0,3)[e] (110,5±0,3)[h]	111,67±0,20 (111,70±0,07)[a] (111,7±0,5)[c] (111,3±0,3)[e] (111,5±0,3)[h]
$K_{T,\phi,2}^{\infty}$, 10^4 cm^3/mol·bar	-15,2±0,7 (-15,03±0,57)[a] (-14,62±0,5)[g] (-14,8±0,1)[h]	-17,3±0,7 (-18,30±1,02)[a] (-17,21±0,5)[g] (-15,6±0,2)[h]	-13,2±2,0 (-14,3±0,50)[a] (-13,09±0,5)[g] (-12,7±0,2)[h]
$K_{S,\phi,prac,2}^{\infty}$, 10^4 cm^3/mol·bar	-18,3±0,7 (-17,8±0,3)[c] (-17,6±0,3)[e] (-17,80±0,01)[f] (-17,80±0,02)[h]	-21,3±0,7 (-20,4±0,4)[b] (-20,8±0,5)[e] (-20,8±0,1)[h]	-15,7±2,0 (-16,0±0,5)[e] (-16,0±0,1)[h]
Hydration number	8,5±0,1 (8,4)[e]	8,7±0,1 (8,7)[e]	8,1±0,3 (8,1)[e]
$\left[\dfrac{\partial K_S^{\infty}}{\partial P}\right]_T \cdot 10^6$cm^{3}mol^{-1}bar^{-2}	1,3±0,1	1,4±0,1	1,1±0,1

[a] Ref. 68, [b] Ref. 22, [c] Ref. 15, [d] Ref. 19, [e] Ref. 17, [f] Ref. 69, [g] Ref. 62, [h] Recommended values by Goldberg and Tewari in Ref. 70.

Partial molar compressions for D-glucose are a bit lower than literature values. It is possible that insufficient drying caused this deviation.

$V_{\phi,2}$ for D-mannose show negative concentration dependence, -3,6 cm^{3}kg·mol^{-2} that is not consistent with the recommended value of 1,2 cm^{3}kg·mol^{-2} given by Høiland[74]. There are several possible causes for this; insufficient drying, slow equilibrium that lead to different conformer composition in each solution, systematic temperature deviations and bacterial growth. One should therefor be cautious discussing data for D-mannose at elevated pressure. For all the other sugars $V_{\phi,2}$ show a small positive concentration dependence. This reflects the favourable hydration of carbohydrates and the idea of carbohydrate-solutions as ideal solutions.

The obtained values at atmospheric pressure agree well with the reported data and hence constitute the foundation for discussion of properties obtained at elevated pressures.

Table 14   Calculated data for D-ribose and L-arabinose at atmospheric pressure. Literature values are given in parenthesis.

	D-ribose	L-arabinose	D-arabinose
V_2^{∞}, cm^3/mol	95,18±0,07 (95,20±0,01)[a] (95,26±0,02)[c] (95,3±0,1)[d] (95,2±0,3)[e] (95,2±0,1)[i]	93,35±0,20 (93,3±0,2)[f] (91,9±0,8)[b] (93,21)[j]	(93,43±0,07)[c] (93,5±0,2)[d] (93,23±0,02)[h] (93,7±0,3)[i]
$K_{T,\phi,2}^{\infty}$, 10^4 cm^3/mol·bar	-9,0±0,9 (-9,22±0,20)[c] (-8,4±0,2)[i]	-16,0±1,5 (-16,31±0,3)[f]	(-16,43±0,51)[c] (-15,2±0,2)[i]
$K_{S,\phi,prac,2}^{\infty}$, 10^4 cm^3/mol·bar	-12,5±1,0 (-12,5±0,5)[e] (-12,4±0,2)[d] (-12,5±0,1)[i]	-19,6±1,5 (-19,0±0,3)[f] (-16,90)[j]	(-19,2±0,1)[d] (-19,3±0,1)[i]
Hydration number	6,8±0,2 (6,8)[d]	7,6±0,2	(7,6)[d]
$\left[\dfrac{\partial K_S^{\infty}}{\partial P}\right]_T$ ·10^6cm^{3}mol^{-1}bar^{-2}	1,2±0,1	1,4±0,1	

[a] Ref. 71, [b] Ref. 15, [c] Ref. 68, [d] Ref. 22, [e] Ref. 17, [f] Ref. 62 [h] Ref. 72, [i] Recommended values by Goldberg and Tewari in Ref. 70.[j] Ref. 73

Values for D-arabinose are also included in Table 14 for comparison with L-arabinose. As seen in Table 1 at page 3, D-arabinose is predominantly present as α-D-arabinopyranose in the inverted chair conformation, $^1C_4$, which is the mirror image of α-L-arabinopyranose in $^4C_1$. Table 14 shows that D- and L- arabinose have similar values.
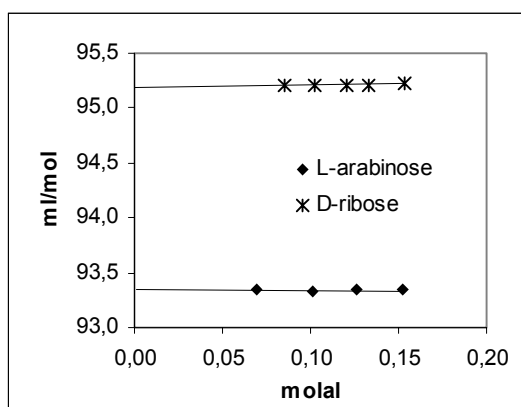
Figure 10 $V_{\phi,2}$ for D-ribose and L-arabinose
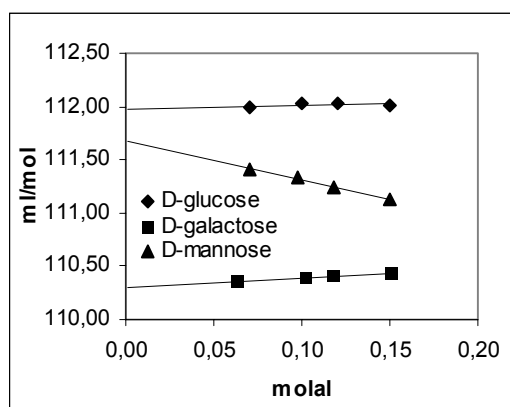
Figure 11 $V_{\phi,2}$ for D-glucose, D-galactose and D-mannose
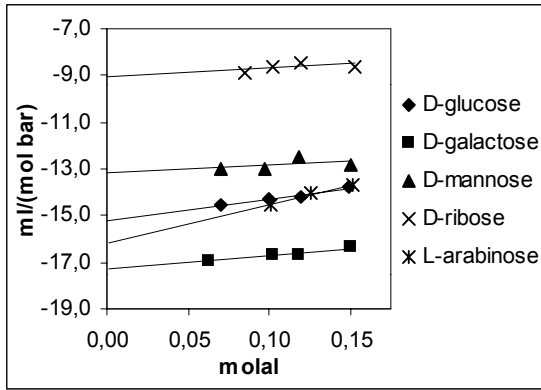
Figure 12 $K_{T,\phi,2}$ as function of concentration
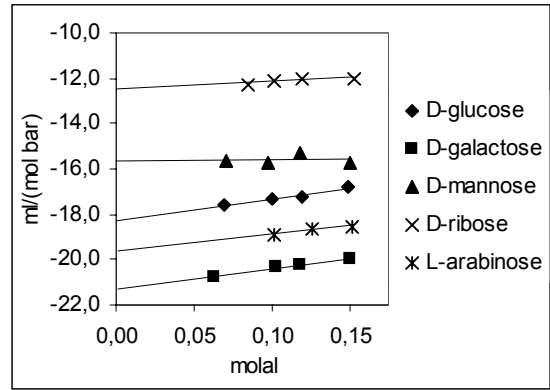
Figure 13 $K_{S,\phi2,prac}$ as   function   of concentration

Figure 12 and Figure 13 show apparent isothermal and isentropic molar compression as function of concentration. There is a larger scatter and different slope in $K_{S,\phi,2,prac}$ for D-mannose. This is probably caused by the deviation in $V_{\phi,2}$ for D-mannose and explains the small somewhat higher value in compression compared to literature data.   L-arabinose show an anomalous $K_{T,\phi,2}$ dependence on concentration which lead to a more negative value compared to literature data. This is probably due to inaccurate expansivities and few data. These possible errors for both L-arabinose and D-mannose continue for all pressures and thus lead to a systematic deviation. However, it is possible to discuss trends in these sugars compared to other, but bearing in mind the high uncertainty in absolute values.

Figure 14 show hydration number as function of concentration.

Limiting values for the pressure derivative of $K_{T,2}^{\infty}$ were not acquired from concentration dependence and thus cannot be plotted as a function of concentration.
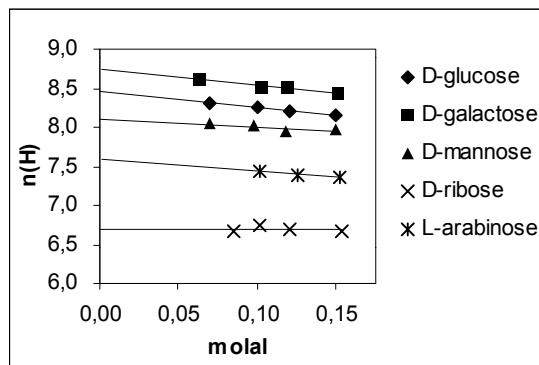
Figure 14 n_H as function of concentration.

4.3 Elevated pressures

In order to use the iterative process, expansion coefficient, α and volume specific heat capacity, σ_p, had to be known for each concentration. See 2.2.1 page 12 for calculation of α from density data. Density for D-glucose, D-galactose, D-mannose and L-arabinose at different temperatures were acquired from the density data of Helland[62] and Holvik[63,17].

Densities for each concentration at the previously measured temperature were estimated with linear regression of third order. Densities for D-ribose were measured at 10, 20, 25 and 35°C. Densities for L-arabinose were measured at 20, 25 and 35°C and data from Helland[62] were used at 10°C.

σ was estimated with first order linear regression from the data of Galema et.al[34].

It was not possible to measure all solutions of each sugar at equal pressures. It was therefore necessary to predict each property at a given pressure to obtain the limiting value. This was done by fitting raw data to a polynomial function of 3rd degree, and then estimate each property for all concentrations at equal pressures.

Data in all figures are fitted to a polynomial function of 2nd degree, which is not a description of the data, but merely a convenient way to see relative trends in the data.

4.3.1 Limiting partial molar volume

Limiting partial molar volume was found by using Equation 39 to calculate apparent molar volume and then extrapolate to zero concentration. Raw data are given in A.IV page 51.

It is important to understand that the limiting partial molar volume is not the molar volume of the solute. V_2^{∞} is the volume change one mole of solute molecules would induce to an ideal solution, that is, no solute-solute interactions, with fixed amount of solvent.
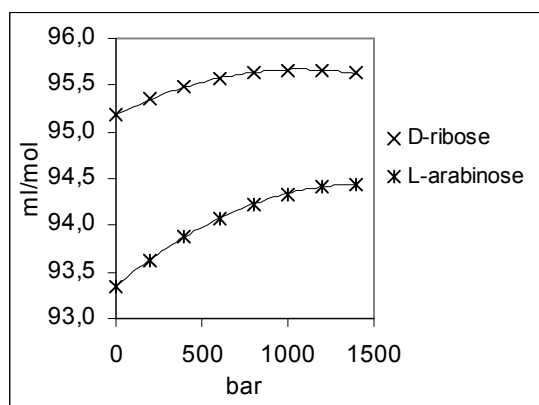
Figure 15 V_2^{∞} as function of pressure for D-ribose and L-arabinose
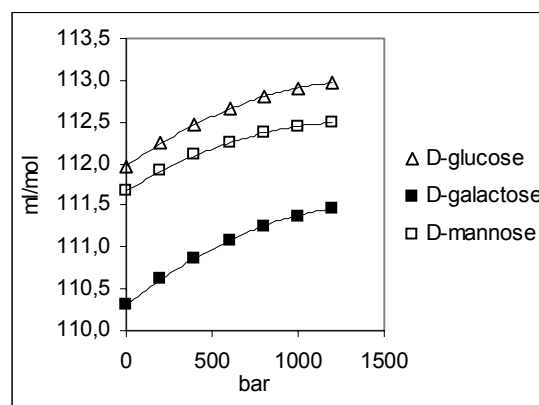
Figure 16 V_2^{∞} as function of pressure for D-glucose, D-galactose and D-mannose

Table 15   Limiting partial molar volume, V_2^∞, in cm^{3}mol^{-1}as function of applied pressure for the investigated carbohydrates.

Applied pressure, bar	D-glucose ±0,10	D-galactose ±0,07	D-mannose ±0,10	D-ribose ±0,07	L-arabinose ±0,20
0	111,97	110,31	111,67	95,18	93,35
200	112,25	110,62	111,91	95,35	93,63
400	112,47	110,87	112,10	95,48	93,88
600	112,66	111,09	112,25	95,58	94,08
800	112,80	111,25	112,37	95,64	94,23
1000	112,90	111,38	112,45	95,66	94,34
1200	112,97	111,47	112,49	95,66	94,41
1400	113,01	111,52	112,50	95,63	94,45

4.3.2 Limiting partial isothermal and isentropic molar compression

Limiting partial isothermal compression, $K_{T,\,2}^\infty$ was calculated from apparent isothermal molar compression, $K_{T,\phi,2}$, using first order linear regression and Equation 25

Both apparent isentropic molar compression, $K_{\phi,S,2}$, and practical apparent isentropic $K_{\phi,S,2,prac.}$, molar compression were calculated from the speed of sound data at atmospheric pressure. The difference was found to be insignificant for all sugars at all concentration, that is, well below the uncertainty. This is probably due to the low concentration and thereof the small difference in the expansion coefficient and volume specific heat compared to pure water. Limiting partial isentropic molar compression, $K_{S,2}^\infty$, was calculated by extrapolating $K_{\phi,S,2,prac.}$ from a first order regression analysis to zero concentration.

Table 16   Limiting partial isothermal molar compression, $K_{T,2}^\infty$, in $10^4 \cdot$cm^{3}mol^{-1}bar^{-1} at applied pressures.

Applied pressure, bar	D-glucose ±0.7	D-galactose ±0,7	D-mannose ±2,0	D-ribose ±0,9	L-arabinose ±1,5
0	-15,2	-17,3	-13,2	-9,0	-16,0
200	-12,6	-14,2	-10,6	-7,6	-13,7
400	-10,2	-11,6	-8,5	-5,8	-11,2
600	-8,1	-9,3	-6,6	-3,9	-8,7
800	-6,1	-7,4	-4,9	-2,0	-6,4
1000	-4,3	-5,5	-3,2	-0,3	-4,4
1200	-2,6	-3,5	-1,4	0,9	-2,6
1400	-0,9	-1,3	0,7	1,4	-1,3

Table 16 and Table 17 list $K_{T,2}^\infty$ and $K_{S,,2}^\infty$, respectively, and displayed together with molar volume of pure water, as function of pressure in Figure 17 and Figure 18. Both $K_{T,2}^\infty$ and $K_{S,2}^\infty$ show the same trends. As pressure increase difference in compression diminish. At zero applied pressure there is a difference in $K_{T,2}^\infty$ of $2,1 \cdot 10^4 \cdot$cm^{3}mol^{-1}bar^{-1} between D-glucose and D-galactose. This difference decrease to $0,4 \cdot 10^4 \cdot$cm^{3}mol^{-1}bar^{-1} at 1400 bars. This is a significant decrease. The decrease, $7,0 \cdot 10^4 \cdot$cm^{3}mol^{-1}bar^{-1} to $2,7 \cdot 10^4 \cdot$cm^{3}mol^{-1}bar^{-1},

also exist for D-ribose and L-arabinose. However, there is not a significant decrease for D-mannose compared to either D-glucose or D-galactose. This might be attributed to the large uncertainties for D-mannose.

Table 17   Limiting partial isentropic molar compression, $K_{S,2}{}^{\infty}$, in $10^4 \cdot cm^3 mol^{-1} bar^{-1}$ at applied pressures.

Applied pressure, bar	D-glucose ±0.7	D-galactose ±0,7	D-mannose ±2,0	D-ribose ±1,0	L-arabinose ±1,5
0	-18,3	-21,3	-15,7	-12,5	-19,6
200	-15,5	-17,9	-12,9	-11,0	-17,0
400	-12,9	-15,1	-10,6	-8,8	-14,2
600	-10,6	-12,6	-8,6	-6,8	-11,6
800	-8,5	-10,5	-6,8	-4,7	-9,2
1000	-6,6	-8,4	-5,0	-3,0	-7,0
1200	-4,8	-6,3	-3,2	-1,6	-5,1
1400	-3,0	-4,0	-1,1	-1,0	-3,6
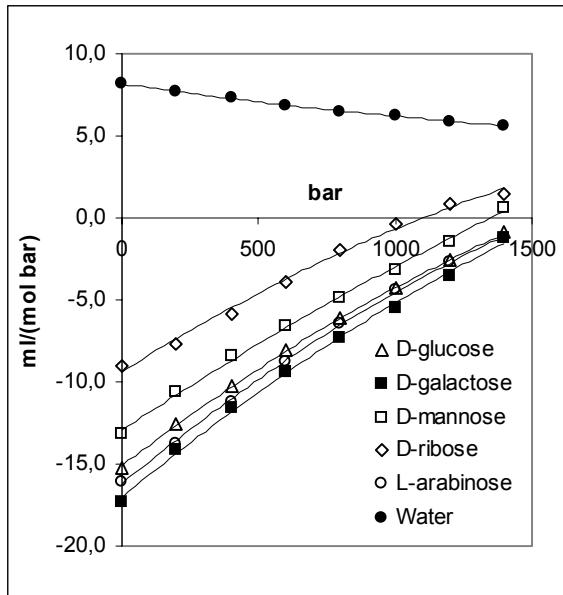
Figure 17 $K_{T,2}{}^{\infty}$ as function of pressure
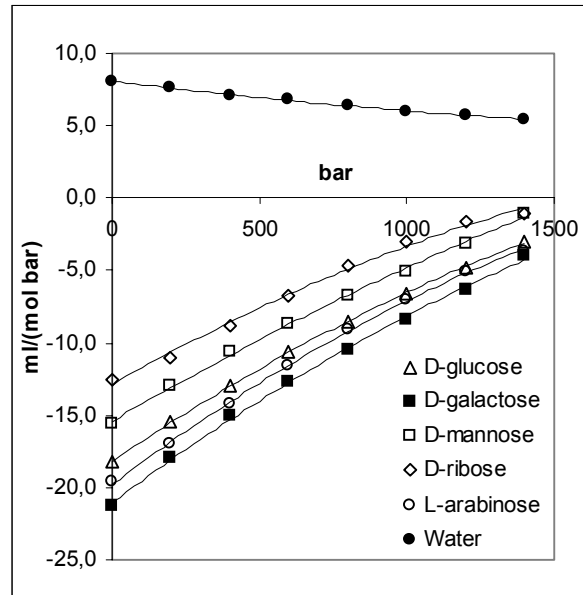
Figure 18 $K_{S,2}{}^{\infty}$ as function of pressure.

4.3.3   Hydration numbers

Hydration numbers were obtained from Equation 43 at page 17 and are given in Table 18 and Figure 20. The hydration numbers decrease as function of pressure, hence fewer water molecules are disturbed by the presence of a solute molecule.

As for compression there is a significant diminishing difference in hydration number between D-glucose and D-galactose, and D-ribose and L-arabinose.

Table 18   Limiting hydration number, n_H.

Applied pressure, bar	D-glucose $\pm 0,1$	D-galactose $\pm 0,1$	D-mannose $\pm 0,3$	D-ribose $\pm 0,2$	L-arabinose $\pm 0,2$
0	8,5	8,7	8,1	6,8	7,6
200	8,3	8,5	7,9	6,8	7,5
400	8,1	8,3	7,8	6,6	7,3
600	8,0	8,2	7,6	6,4	7,1
800	7,8	8,0	7,5	6,2	6,8
1000	7,6	7,8	7,3	6,0	6,6
1200	7,4	7,6	7,1	5,8	6,4
1400	7,2	7,2	6,8	5,8	6,2
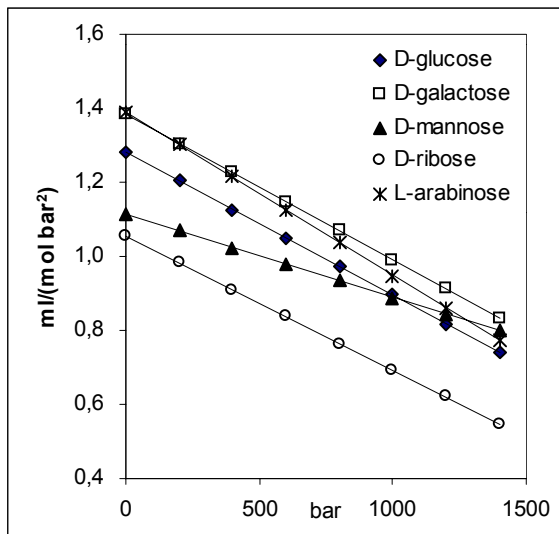
Figure 19 $\left[\dfrac{\partial K_{T,2}{}^{\infty}}{\partial P} \right]_T$ as function of pressure
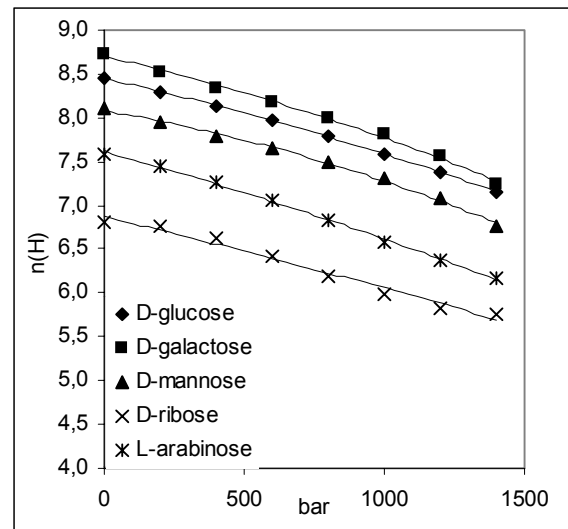
Figure 20 n_H as   function   of   pressure

4.3.4 Pressure derivative of limiting partial isothermal molar compression

The pressure derivative of partial molar compression was found by fitting $K_{T,2}{}^{\infty}$ to a polynomial function of 2nd degree, followed by derivation of this function with respect to pressure. This property was thus not calculated at a given concentration and is therefore not a "true" limiting property. The calculated values are given in Table 19 and displayed in Figure 19.

As seen in Figure 19, D-mannose behaves differently from the other sugars. The reason for this might be the large concentration dependence of $V_{\phi,2}$ and thus larger error.

Differences in pressure derivative of partial isothermal are small but significant.

Since the obtained values are calculated by differentiation of a 2nd order polynomial function , it is obvious that these are linear with respect to pressure. This linearity is thus not experimentally observed. However, the decrease suggests that rate of increase in partial molar compression as pressure rise, decrease. In more simple words; $K_{T,2}{}^{\infty}$ is concave down.

36

Table 19 Pressure derivative of the limiting partial molar compression, $\left[\dfrac{\partial K_T^{\infty}}{\partial P}\right]_T$, in $10^6 \cdot cm^3 mol^{-1} bar^{-2}$ at applied pressures.

Applied pressure, bar	D-glucose ±0,1	D-galactose ±0,1	D-mannose ±0,1	D-ribose ±0,1	L-arabinose ±0,1
0	1,3	1,4	1,1	1,1	1,4
200	1,2	1,3	1,1	1,0	1,3
400	1,1	1,2	1,0	0,9	1,2
600	1,0	1,1	1,0	0,8	1,1
800	1,0	1,1	0,9	0,8	1,0
1000	0,9	1,0	0,9	0,7	0,9
1200	0,8	0,9	0,8	0,6	0,9
1400	0,7	0,8	0,8	0,5	0,8

4.4 Interpretation of results

In order to interpret the results it is useful to review partial molar compression. Mathematically, partial molar compression is the negative pressure derivative of partial molar volume. For most solutes K_2 is negative, which means that partial molar volume increase with increasing pressure. A negative compression might seem illogical. How can a volume increase as pressure increase? To answer this question one must look at the structuring of water to a solute molecule. A solute molecule will in most cases, and especially for a carbohydrate, induce a higher degree of structure to adjacent water molecules. These water molecules are said to comprise the hydration shell. The word shell is a bit misleading in the sense that the structure of water molecules is not a spherical shell, but is highly anisotropic and specific to functional groups at the solute molecule. The hydration shell consists of regions of higher and lower water density than bulk water caused by specific hydrogen bonding between adjacent water molecules and, if possible, the solute molecule[13]. As pressure increase this structure is broken down. This leads to a lower hydration shell density and thereof a larger hydration shell volume.

The modified stereo specific hydration model of Galema[22,31,32,34,35] depicts the hydration of carbohydrates to be depending on the relative positions of the hydroxyl groups at carbon 2 and carbon 4. Table 20 places the investigated monosaccharides in the predicted group in the modified stereo-specific hydration model. Unfortunately, none of the investigated monosaccharides belong to group 1. The investigated sugars do not deviate from this model.

Table 20 The modified stereo-specific hydration model

	Group 1	Group 2	Group 3
Position of OH(2)	axial	axial or equatorial	equatorial
Position of OH(4)	axial	equatorial	axial
$K_{T,2}^{\infty}$ and $K_{S,2}^{\infty}$	least negative	intermediate negative	most negative
Fit to water	Best	Intermediate	Poorest
Investigated sugars	None	D-glucose, 1e2e3e4e6e D-mannose, 1a2a3e4e6e D-ribose, 1e2e3a4e	D-galactose, 1e2e3e4a6e L-arabinose, 1e2e3e4a

D-galactose has a lower $K_{T,2}^{\infty}$ than D-glucose and D-mannose, and L-arabinose has a lower $K_{T,2}^{\infty}$ than D-ribose. This order continues as pressure increase. This is an indication of stereo specific hydration at high pressure. However, there is a diminishing difference in $K_{T,2}^{\infty}$ between the investigated aldopentoses and aldohexoses. This effect is most clear for D-ribose and L-arabinose where the difference is 7,0 $cm^3mol^{-1}bar^{-1}$ at atmospheric pressure and 2,7 $cm^3mol^{-1}bar^{-1}$ at 1400 bar. This is an indication of less stereo-specific hydration with increasing pressure. It would be interesting to measure if this has any effect on the kinetic medium effects studied by Galema et.al[31,32]. It is also possible that reactions that are hindered at atmospheric pressure because of the specific hydration of carbohydrates are possible at high pressure because of altered hydration.

The large change in $K_{T,2}^{\infty}$, with rising pressure stand in contrast to the relatively small change in hydration number n_H. This can be interpreted as even though the hydration shell structure is broken down with rising pressure there still remains some structure, which comprise a larger volume.

There is little gain in information from the pressure derivative of $K_{T,2}^{\infty}$, which is a measure of inclination of $K_{T,2}^{\infty}$. As expected L-arabinose, which has the highest $K_{T,2}^{\infty}$ of the measured pentoses, has the lowest inclination. The same trend is observed for aldopentoses. The pressure derivative of $K_{T,2}$ decrease with decreasing pressure, hence $K_{T,2}$ is not linear with pressure, but concave down. This suggests that the effect of increasing pressure on the hydration layer diminish as pressure increase. It is possible that the pressure derivative will be sensitive for different kinds of hydration so that hydration of ionic solutes, apolar solutes and polar solutes will have values within specific ranges.

Little is known about change in equilibrium of anomers as function of change in pressure. O'Connor et.al. studied mutarotation of D-glucose at high pressure and found the equilibrium constant $K_{eq}=k_{\alpha}/k_{\beta}$ to be nearly unchanged from the 1,7 found at 1 bar. It is not possible to gain any information about equilibrium of the other investigated sugars from the results presented here. Equilibrium of D-ribose differs from the other investigated monosaccharides (see Table 1 page3). Aqueous solutions of D-ribose consists of α- and β-D-ribopyranose, which is present in both $^{4}C_{1}$ and $^{1}C_{4}$, and α- and β-D-ribofuranose. The proportion of the dominant conformer, β-D-ribopyranose in $^{4}C_{1}$, is only 41 %. For all the other investigated sugars this proportion is 60% or higher. However, this does not seem to affect the hydration of D-ribose with rising pressure differently compared to the other investigated sugars. In general has no anomalous behaviour, caused by changes in pressure, of any sugar compared to the other sugars been observed. This suggests that the same effects for all sugars cause changes in hydration.

An interesting question arise as partial isothermal molar compression becomes zero. At zero partial molar compression a perturbation in pressure will not lead to a change in partial molar volume. Yet, the total volume will decrease with increasing pressure because of more dense packing of bulk water molecules. Attempts have been made to divide V_2 and $K_{T,2}$ into distinct terms[42]

Equation 59
$$K_{T,\phi,2} = K_{T,i} + n_h \left(\overline{K}_{T,h} - \overline{K}_T^{\;*} \right)$$

In Equation 59 $K_{T,i}$ is the intrinsic partial molar compression (assumed to be zero), $\overline{K}_{T,h}$ is partial molar compression of a hydration water molecule, $\overline{K}_T^{\;*}$ is partial molar compression of a bulk water molecule and n_h is number of molecules in hydration shell. A problem with Equation 59 is that by using this equation on pure water(solute) in water(solvent), a partial molar compression of zero will be the result. But water has a molar compression of 8,17 $cm^3 mol^{-1} bar^{-1}$. A solute that has positive $K_{T,\phi,2}$ will according to Equation 59 have a more compressible hydration shell the bulk of solution, which is in contradiction to other results[75].

It is here believed that at zero partial molar compression the volume gain caused by breaking of hydration shell structure is cancelled by a more dense packing of water molecules in the hydration shell. Zero $K_{T,2}$ is thus not particularly interesting from a thermodynamic view. At zero $K_{T,2}$ the intrinsic part of $K_{T,2}$ also contributes significantly to $K_{T,2}$. However, this only means that the measured pressures of zero $K_{T,2}$ are a bit lower than the measured ones.

Following the lead depicted above one might expect $K_{T,2}$ to reach a maximum and then decrease in the same rate as bulk water (see Figure 12) Unfortunately, speed of sound measurements were not conducted at such high pressures.

5 Conclusion

Partial molar volume, limiting partial molar isentropic and isothermal compression, hydration numbers and pressure derivative of compression have been acquired by means of speed of sound measurements at elevated pressure and density measurements at atmospheric pressure.

The results show clear indications of altered hydration with increasing pressure.

The difference between $K_{S,\phi,2,\text{prac.}}$ and $K_{S,\phi,2}$ is negligible in dilute aqueous monosaccharide solutions.

The pressure derivative of $K_{T2,}{}^{\infty}$ does not contribute to new information about stereo specific hydration of monosaccharides.

References

1. J.L. Green and C.A. Angell *J.Phys.Chem.* **1989**, 93, 2880
2. I. Gill and R. Valivety *Angew. Chem. Int. Ed.* **2000**, 39 nr 21, 3802
3. V. Ringnes in *Navn på kjemiske stoffer*, Cappelen, 1st ed, Oslo **1996**, page 118
4. Peter Collins and Robin Ferrier in: *Monosaccharides*, Wiley, Chichester England **1995**, page 27.
5. F. Franks, J.R. Grigera in: *Water science reviews. 5*, F. Franks, Ed., Cambridge University Press, Camebridge **1990**, ch. 4.
6. F.Franks, P.J. Lillford and G. Robinson *J.Chem.Soc.Faraday Trans. I* **1989**, 85(8), 2417
7. S.J. Angyal and V.A. Pickles *Aust.J.Chem.* **1972**, 25, 1695
8. S.J. Angyal *Angew.Chem.* **1969**, 81, no 5, 172
9. M. Rudrum *J.Chem.Soc* **1965**, 1, 52
10. S.J. Angyal and V.A. Pickles *Aust.J.Chem.* **1972**, 25,1695
11. S.J. Angyal and G.S. Bethell *Aust.J.Chem.* **1976**, 29,1249
12. C.J. O'Connor, A.L. Odell and A.A.T. Bailey *Aust.J.Chem.* **1983**, 36, 279
13. Q. Liu, J.W. Brady *J.Am.Chem.Soc.* **1996**, 118,12276
14. J.T. Edward and P.G. Farrell *Can.J.Chem.* **1975**, 53, 2965
15. F. Shahidi, P.G. Farrell and J.T. Edward *J.Sol.Chem* **1976**, 5, 807
16. L. Lepori and P. Giannim *J.Sol.Chem.* **2000**, 29(5), 405
17. H. Høiland, H. Holvik *J.Sol.Chem.* **1978**, 7(5), 587
18. H. Høiland, in *Thermodynamic Data for Biochemistry and Biotechnology*, H.-J. Hinz, ed., Springer, Berlin **1986** ch. II.4
19. F. Franks, J.R. Ravenhill and D.S. Reid *J.Sol.Chem.* **1972**, 1(1), 3
20. M.J. Blandamer *J.Chem.Soc. Faraday Trans.* **1998**, 94, 1057
21. M.J. Blandamer *Chem.Soc.Rev.* **1998**, 27, 73
22. S.A. Galema and H. Høiland, *J.Phys.Chem* **1991**, 95, 5321
23. F. Franks *Pure & Appl. Chem.* **1987**, 59(9), 1189
24. M.A. Kabayama, D. Patterson and L Piche *Can.J.Chem.* **1958**, 36, 557
25. M.A. Kabayama and D. Patterson *Can.J.Chem.* **1958**, 36, 563
26. M.J. Tait, A. Suggett, F. Franks, S. Ablett and P.A. Quickenden *J.Sol.Chem.* **1972**, 1(2), 131
27. D.T. Warner *Nature* **1962,** 196, 1055
28. F. Franks, D.S. Reid and A. Suggett *J.Sol.Chem.* **1973**, 2, 99
29. A. Suggett *J.Sol.Chem.* **1976**, 5, 33
30. A. Suggett and A.H. Clark *J.Sol.Chem.* **1976**, 5, 1
31. S.A. Galema, M.J. Blandamer and J.B.F.N. Engberts *J.Am.Chem.Soc.* **1990**, 112, 9665
32. S.A. Galema, M.J. Blandamer and J.B.F.N. Engberts *J.Org.Chem* **1992**, 57, 1995
33. W. Blokzijl, J.B.F.N. Engberts and M.J. Blandamer *J.Am.Chem.Soc.* **1990**, 112, 1197
34. S.A. Galema, J.B.F.N. Engberts, H. Høiland, G.M. Frøland *J.Phys.Chem.* **1993**, 97,6885
35. S.A. Galema, E. Howard, J.B.F.N. Engberts and J.R. Grigera *Carbhydrate Res.* **1994**, 265(2), 215
36. B. Leuroux, H. Bizot, J.W. Brady and V. Tran *Chem.Pys.* **1997**, 216, 349
37. Q. Liu, R.K. Schmidt, B. Teo, P.A. Karplus and J.W Brady *J.Am.Chem.Soc* **1997**, 119, 7851
38. C. Molteni and M. Parrinello *J.Am.Chem.Soc.* **1998**, 120, 2168
39. Q. Liu and J.W. Brady, J.Phys.Chem. B, **1997**, 101, 1317
40. J. Behler, D.W. Price and M.G.B. Drew *Phys.Chem.Chem.Phys.* **2001**, 3, 588
41. K.S. Sidhu, J.M. Goodfellow and J.Z. Turner *J.Chem.Phys.* **1999**, 110(16), 7943
42. T.V. Chalikian, A.P. Sarvazyan, T. Funck, C.A. Cain and K.J. Breslauer *J.Phys.Chem.* **1994**, 98, 321
43. E. Vikingstad, A. Skauge and H. Høiland *J.Coll.Int.Sci.* **1979**, 72(1), 59
44. T. Maldal *Hovedfagsoppgave; Partielle molare volum og kompressibiliteter som funksjon av trykk og temperatur av natrium-dodecyl-sulfat og n-alkholblandinger* University of Bergen **1984**
45. A.P. Sarvazayan *Annu.Rev.Biophys.Chem.* **1991**, 20, 321
46. T.V. Chalikian, A.P. Sarvazyan, K.J. Breslauer *Biophys.Chem.* **1994**, 51, 89
47. J.C.R. Reis *J.Chem.Soc. Faraday Trans. 2* **1982**, 78, 1595

48. Harned and Owen, *The Physical Chemistry of Electrolytes Solutions, Reinhold*, New York, 3rd edn **1958**, section 8.7
49. A. B.Wood, *A textbook of sound* G Bell and Sons, **1941**
50. C.-T. Chen, R.A. Fine and F.J. Millero *J.Chem.Phys.* **1977**, 66(5), 2142
51. L.A. Davis and R.B. Gordon *J. Chem. Phys.* **1967**, 46(7), 2650
52. J.L. Daridon, A. Lagrabette and B. Lagourette *J.Chem.Thermodynamics* **1998**, 30, 607
53. S.P. Moulik and S. Gupta *Can.J.Chem.* **1989**, 67, 356
54. J.O.M. Bockris, and A.K.N. Reddy, in *Modern Electrochemistry*; Plenum: New York, **1977** Vol I, p 127.
55. R. Garnsey, R. J. Boe, R. Mahoney and T. A. Litovitz *J.Chem.Phys.* **1969**, 50, 5222
56. E. Høgseth, G. Hedwig and H. Høiland *Rev.Sci.Inst.* **2000**, 71(12)
57. V. A. Del Grosso and C. W. Mader *J.Acoust.Soc.Am.* **1972**, 5, 1442
58. W.D. Wilson *J.Acoust.Soc.Am.* **1959**, 31(8), 1067
59. C. –T. Chen and F. T. Millero *J. Acoust. Soc. Am.* **1976**, 60(6), 1270
60. CRC, *Handbook of Chemistry and Physics*, ed. David R. Lide, 76th edition, **1995**
61. G. S. Kell *J.Chem.Eng.Data* **1975**, 20, 97
62. K. Helland, *Hovedfagoppgave; Hydratasjon av karbohydrater. ,* Universitetet i Bergen, **1997**
63. H. Holvik in *Hovedfagoppgåve; Partielle molale volum og partielle molale kompressibilitetar av karbohydrat løyste i vatn.*, Universitetet i Bergen, **1977**
64. A.H. Smith and A.W. Lawson *J.Chem.Phys* **1954**, 22, 351
65. T.A. Litovitz and E.H. Carnevale *J.Appl.Phys.* **1955**, 26, 816
66. H. Sato, K. Watanabe, J.M.H. Levelt Sengers, J.S. Gallagher, P.G. Hill, J. Straub and W. Wagner *J.Phys.Chem.Ref.Data* **1991**, 20(5), 1023
67. R. Hillbert *Phys.Chem* **1981**, 85, 636
68. P.K. Banipal, T.S. Banipal, B.S. Lark and J.C. Ahluwalia *J.Chem.Soc*. Faraday Trans. **1997**, 93(1), 81
69. P.J. Bernal, W.A. Van Hook *J.Chem.Thermodyn.* **1986**, 18, 955.
70. R.N. Goldberg and Y.B. Tewari *J.Phys.Chem.Ref.Data* **1989**, 18(2), 809
71. H. Uedaira and H.Uedaira *J.Sol.Chem.* **1985**, 14(1), 27
72. K. Zhuo, J. Wang, Y. Yue and H. Wang *Carb.Res.* **2000**, 328, 383
73. G.G. Birch, S. Parke, R. Siertsema and J.M Westwell *Pure & Appl. Chem.* **1997**, 69(4), 685
74. H. Høiland, in *Thermodynamic Data for Biochemistry and Biotechnology*, H.-J. Hinz, ed., Springer, Berlin, **1986** ch.II.2
75. C. Wakai, N. Matubayasi and M. Nakahara *J.Phys.Chem. A* **1999**, 103(34), 6686

Appendices

A.I List of symbols and variables

Symbol	Meaning	
V_2	Partial molar volume of solute	$cm^3 \cdot mol^{-1}$
V_1	Partial molar volume of solvent	$cm^3 \cdot mol^{-1}$
V_1^*	Molar volume of pure solvent	$cm^3 \cdot mol^{-1}$
$V_{\phi,2}$	Apparent partial molar volume	$cm^3 \cdot mol^{-1}$
V_2^∞	Limiting partial molar volume	$cm^3 \cdot mol^{-1}$
V_w	Intrinsic volume	
V_e	Interaction volume	
$K_{T,2}$	Partial isothermal compression	$cm^3 \cdot mol^{-1} \cdot bar^{-1}$
$K_{T,\phi,2}$	Apparent isothermal molar compression	$cm^3 \cdot mol^{-1} \cdot bar^{-1}$
$K_{T,2}^\infty$	Limiting partial molar compression	$cm^3 \cdot mol^{-1} \cdot bar^{-1}$
$K_{S,2}$	Partial isentropic molar compression	$cm^3 \cdot mol^{-1} \cdot bar^{-1}$
$K_{S,\phi,2}$	Apparent isentropic molar compression	$cm^3 \cdot mol^{-1} \cdot bar^{-1}$
$K_{S,\phi,2,,prac}$	Practical apparent isentropic molar compression	$cm^3 \cdot mol^{-1} \cdot bar^{-1}$
$K_{S,2}^\infty$	Limiting partial isentropic molar compression	$cm^3 \cdot mol^{-1} \cdot bar^{-1}$
$K_{X,\phi,2}$	$K_{T,\phi,2}$ and $K_{S,\phi,2}$	$cm^3 \cdot mol^{-1} \cdot bar^{-1}$
κ	compressibility	bar^{-1}
n_1	moles of solvent	mol
n_2	moles of solute	mol
p	pressure	bar
m	molality	$mol \cdot kg^{-1}$
ρ	density of solution	$g \cdot cm^{-3}$
ρ^*	density of pure solvent	$g \cdot cm^{-3}$
m_m	mass of solute	g
M_m	molar mass	$mol \cdot kg^{-1}$
T	Temperature or time in density measurements	°C or seconds
t	time	seconds
E_2	partial molar expansion	$cm^3 \cdot mol^{-1} \cdot K^{-1}$
$E_{\phi,2}$	apparent molar expansion	$cm^3 \cdot mol^{-1} \cdot K^{-1}$
E_2^∞	Limiting partial molar expansion	$cm^3 \cdot mol^{-1} \cdot K^{-1}$
α	expansivity	K^{-1}
u	speed of sound	$m \cdot s^{-1}$
σ_p	volume specific heat capacity	$bar \cdot K^{-1}$
γ	adiabatic constant for solution	dimensionless
γ^*	adiabatic constant for pure solvent	dimensionless
n_H	hydration number obtained from κ_S	dimensionless
n_h	number of molecules in hydration shell	dimensionless
n_w	mole fraction of water	dimensionless
n_s	mole fraction of solute	dimensionless
τ	delay	seconds
B	air pressure	torr

e	vapour pressure of water	kPa
F	relative air humidity	dimensionless
g	gravitational constant	$m \cdot s^{-2}$
w	kilogram force per square centimetre	$1\ kp \cdot cm^2 = 0{,}980668\ bar$
$t_{\alpha/2}$	student's t value	
s	length of ultrasonic cell	meter

A.II Operation manual

A.II.1 Speed of sound equipment for measurements at applied pressures.

A.II.1.1   Preparations

Make sure that the cells are not filled with solution from previous experiments.
Use one cell for water reference. Due to dampening of signal in solutions it is advisable to use the cell with the weakest signal.
The timer, a Philips PM 6666, used to measure the time for one cycle by default set the read level in auto. This has to be changed to a defined level. Note that the timer will reset to auto level when power is shut of.

A.II.1.2   Filling of cells

- Use 5 ml syringes or larger.
- Heat the desired solution to 30 – 40°C before injection. This is to reduce chance of bubbles forming at the interior cell wall. If bubbles still appear try to make solution air-free by pulling the syringe so that vacuum arise.
- Rinse the syringe and the cell with small amounts of solution.
- Slowly inject the solution in the rubber-tube screw hole while levelling the other screw hole (see figure). Inject until solution runs out of the other hole. This procedure is for non-surfactant solutions where the interior of the cell, and especially the rubber hose, is not wetted by the solution. If the solution is wetting care must be taken so that air bubbles are not forced into the cell.
- When the cell is filled with solution close the hole at the top of the cell.
- Check the signal at the oscilloscope. Gently knock the cell. If the signal is unstable or differs from its normal appearance empty the cell and fill it again. Ensure that the signal is strong, that it is at least two echoes. The signal normally weakens at higher pressures and a weak signal at atmospheric pressure may lead to erroneous speed of sound or no signal at all.
- Tighten the other screw and wipe the cell dry. If the cell is not wiped dry, water will sink to the bottom of the pressure vessel where fungus and bacteria might grow and clog the piping.
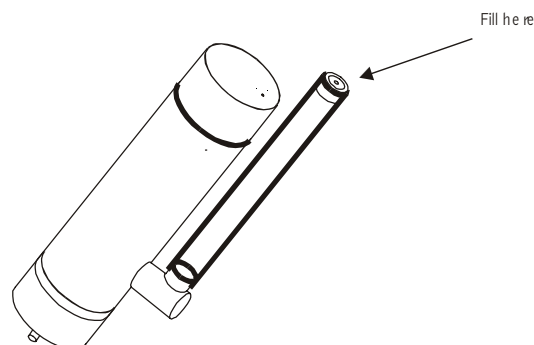
Figure 21   Filling of ultrasonic cell

A.II.1.3 Measurements

- Place up to three cells in rack for pressure measurements or rack for check measurements.
- Turn the selector at the top of the pressure vessel to switch between cells.
- Press the stop button and then the start button to start the signal
- Allow one hour for thermostating. Read of the timer the total time for one cycle. Equilibrium is obtained when this time is constant.

Sometimes signal fails to transmit at a given pressure. Try to reduce or elevate the pressure 10 bars followed by thermostating.
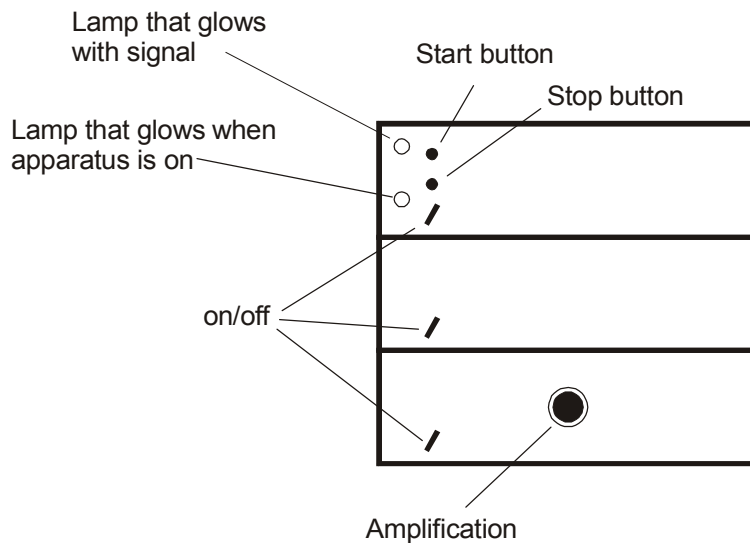
Figure 22   Schematic representation of speed of sound equipment.

A.II.1.4 After use

- Wash the inside and outside of each cell with tempered water and a mild soap solution.
- Rinse the inside with a mild soap solution and water two times and then thoroughly with distilled water.

A.II.2 Instruction in use of high pressure equipment
- Use protecting glasses.
- The hydraulic oil used (Rando HDZ15 from Texaco/Hydro) is very hard to clean off. Use therefore a laboratory coat or other suited clothing.
- The system is designed to bear pressures up to 2000 bar
- Always wipe of exterior water on measure cells.
- Ensure that the o-ring at the bottom of the pressure vessel lid is in place.
- Close the pressure vessel with the brass cylinder and use a metal rod as handgrip.

Valve A is the valve at the right side of the pump. Valve B is the valve under the manometer. See Figure 23

CAUTION! NEVER OPEN THE PUMP-VALVE (VALVE A) UNLESS THE VALVE BELOW THE MANOMETER (VALVE B) IS CLOSED!

A.II.2.1 Elevation of pressure
- Close valve A by turning it clockwise.
- Ensure that valve B is open by closing it and then opening it by turning the handle one counter-clock rotation.
- Pump up to desired pressure with the pressure pump. If start pressure is atmospheric pressure it takes at least 10 pumps till pressure starts rising.
- Close valve B when the desired pressure is obtained. Pressure will drop approximately 20 bar until equilibrium is reached.
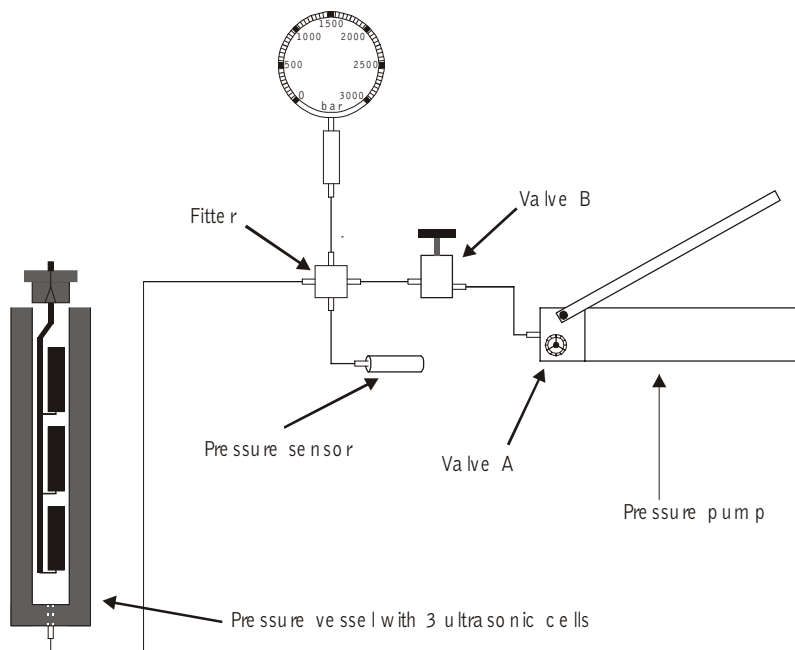
Figure 23   Schematic representation of pressure piping

A.II.2.2   Lowering of pressure

- Ensure that valve B is closed. VERY IMPORTANT!
- Open valve A with one counter-clockwise rotation
- **Slowly** open valve B until pressure drops. If pressure drops to fast there is a greater chance of hysterisis.
- Close valve B and A.
- Pressure will rise approximately 20 bar until equilibrium is reached.

A.II.2.3   Opening of pressure vessel

- Ensure that applied pressure is zero and that both valve A and B are open.
- Use the brass cylinder and the metal rod to open the cover. Give a short "knock" at the end of the metal rod to open and then unscrew the cover counter-clockwise.

A.III Calibration data

A.III.1 Calibration of pressure sensor

Table 21   Calibration data for pressure sensor.

Kilogram force/square centimetre	Pressure/ bar	Voltage /mV	Residual measured vs. predicted. /bar
0	0,0	0,000	0,0
150	147,1	1,477	0,6
160	156,9	1,574	0,5
170	166,7	1,669	0,3
180	176,5	1,769	0,4
190	186,3	1,866	0,3
200	196,1	1,963	0,2
300	294,2	2,943	0,0
350	343,2	3,432	-0,1
550	539,4	5,393	-0,3
750	735,5	7,359	-0,2
950	931,6	9,324	-0,2
1150	1127,8	11,293	0,0
1300	1274,9	12,770	0,0
1500	1471,0	14,740	0,0
1700	1667,1	16,711	0,1
1900	1863,3	18,683	0,2
1950	1912,3	19,176	0,2
1900	1863,3	18,679	-0,2
1850	1814,2	18,189	0,1
1750	1716,2	17,204	0,2
1550	1520,0	15,230	-0,2
1350	1323,9	13,260	-0,2
1150	1127,8	11,292	-0,2
950	931,6	9,325	-0,2
750	735,5	7,359	-0,1
550	539,4	5,397	0,1
350	343,2	3,436	0,3
300	294,2	2,944	0,2
250	245,2	2,453	0,2
200	196,1	1,963	0,2
150	147,1	1,476	0,5
0	0,0	0,000	0,0

The pressure sensor was calibrated with a dead-weight pressure gauge tester. Applied pressure in bars was fitted to measured voltage, U, minus voltage at zero applied pressure, U(0), using second order linear regression.

Equation 60 $$p - p(0) = a_1 \left(U - U(0) \right) + a_2 \left(U - U(0) \right)^2$$

Applied pressure was calculated from applied kilogram force per square centimetre, kp/cm^2 with

Equation 61
$$p = w \cdot g$$

where w is kilogram force per square centimetre and g is the gravitational constant.

	a_1	a_2	R^2	g
	100,0411	-0,0161739	0,99999985	0,980665 m·s-2
Standard error, S_a	0,018	0,0011		

A.IV Data

A.IV.1 Constants

Table 22   Constants used in this thesis

Temperature, °C	10	20	25	35
$\rho^{*\,a}$, g·cm^{-3}	0,9997026	0,9982071	0,997048	0,9940349
$\alpha^{*\,a}$, K^{-1}	0,00008797	0,00020678	0,00025721	0,00034573
$u^{*\,b}$, cm·s^{-1}			1496,687	
σ_p^{*}, bar·K^{-1}			41,669	
τ, µs			1,62±0,01	
M_m hexoses, g·mol^{-1}			180,156	
M_m pentoses, g·mol^{-1}			150,12	

[a] Ref. 61, [b] Ref. 57

A.IV.2 Raw data

Errors for all properties at elevated pressure are equal to those at atmospheric pressure.

Table 23   Measured data for D-glucose at atmospheric pressure and 25°C

molality±0,0001, mol·kg^{-1}	$\rho \pm 4 \cdot 10^{-6}$, g·cm^{-3}	u±0,04, m·s^{-1}	α, K^{-1}	$\sigma_p \pm 0,01$, bar·K^{-1}
0,07002	1,001793	1501,02	0,0002617	41,583
0,10033	1,003821	1502,87	0,0002635	41,546
0,12004	1,005133	1504,08	0,0002647	41,521
0,14970	1,007100	1505,82	0,0002664	41,485

Table 24   Calculated data for D-glucose at atmospheric pressure and 25°C.

molality, mol·kg^{-1}	$V_{\phi,2}$, cm^3·mol^{-1}	$K_{S,\phi,2, prac} \cdot 10^4$, cm^{3}mol^{-1}bar^{-1}	$K_{T,\phi,2} \cdot 10^4$, cm^{3}mol^{-1}bar^{-1}	$n_H \pm 0,1$
0,07002	111,98 (0,07)	-17,59 (0,43)	-14,55 (0,51)	8,31
0,10033	112,02 (0,05)	-17,31 (0,30)	-14,28 (0,35)	8,25
0,12004	112,03 (0,04)	-17,20 (0,25)	-14,18 (0,30)	8,22
0,14970	112,02 (0,03)	-16,81 (0,20)	-13,81 (0,24)	8,14

Table 25   Raw data for D-Glucose at applied pressures

molality mol·kg^{-1}	p, bar	u, m·s^{-1}	γ	ρ, g·cm^{-3}	$V_{\phi,2}$, cm^3·mol^{-1}	$K_{S,\phi,2,prac.}$, cm^3·mol^{-1}·bar^{-1}	$K_{T,\phi,2}$, cm^3·mol^{-1}·bar^{-1}
0,07002	0,0	1501,02	1,01108	1,001793	111,98	-0,001755	-0,001452
	202,7	1535,03	1,01365	1,010696	112,25	-0,001471	-0,001188
	401,5	1568,39	1,01648	1,019077	112,46	-0,001223	-0,000958
	602,3	1602,00	1,01953	1,027211	112,64	-0,000993	-0,000743
	800,3	1635,00	1,02263	1,034930	112,76	-0,000794	-0,000557
	999,7	1668,00	1,02576	1,042419	112,86	-0,000613	-0,000388
	1198,6	1700,57	1,02879	1,049621	112,92	-0,000425	-0,000209
	1399,4	1733,10	1,03169	1,056641	112,94	-0,000273	-0,000065
0,10033	0,0	1502,87	1,01130	1,003821	112,02	-0,001727	-0,001424
	200,4	1536,61	1,01383	1,012605	112,29	-0,001506	-0,001224
	400,9	1570,26	1,01669	1,021041	112,51	-0,001258	-0,000994
	600,7	1603,68	1,01972	1,029117	112,69	-0,001022	-0,000773
	800,1	1636,83	1,02285	1,036876	112,82	-0,000790	-0,000553
	999,6	1669,77	1,02598	1,044353	112,91	-0,000587	-0,000361
	1201,1	1702,74	1,02905	1,051634	112,97	-0,000409	-0,000193
	1399,6	1734,88	1,03191	1,058560	112,99	-0,000267	-0,000058
0,12004	0,0	1504,07	1,01144	1,005133	112,03	-0,001715	-0,001414
	202,7	1538,08	1,01400	1,014004	112,29	-0,001433	-0,001152
	401,5	1571,44	1,01683	1,022355	112,50	-0,001190	-0,000926
	602,3	1605,00	1,01989	1,030460	112,66	-0,000954	-0,000705
	800,3	1637,98	1,02299	1,038154	112,78	-0,000756	-0,000520
	999,7	1670,92	1,02612	1,045618	112,87	-0,000570	-0,000345
	1198,6	1703,44	1,02915	1,052798	112,92	-0,000397	-0,000182
	1399,4	1735,92	1,03205	1,059797	112,94	-0,000250	-0,000042
0,14970	0,0	1505,81	1,01164	1,007100	112,02	-0,001377	-0,001677
	200,4	1539,53	1,01418	1,015853	112,27	-0,001153	-0,001433
	400,9	1573,15	1,01703	1,024260	112,48	-0,000918	-0,001181
	600,7	1606,54	1,02007	1,032310	112,64	-0,000704	-0,000952
	800,1	1639,68	1,02320	1,040044	112,76	-0,000503	-0,000738
	1201,1	1705,53	1,02939	1,054757	112,89	-0,000168	-0,000383
	1399,6	1737,60	1,03226	1,061663	112,91	-0,000031	-0,000239

Table 26   Measured data for D-galactose at atmospheric pressure and 25°C

molality±0,0003, mol·kg^{-1}	ρ±4·10^{-6}, g·cm^{-3}	u±0,04, m·s^{-1}	α, K^{-1}	σ_p±0,01, bar·K^{-1}
0,06346	1,001454	1500,80	0,0002626	41,5851
0,10279	1,004152	1503,30	0,0002653	41,5326
0,11873	1,005236	1504,32	0,0002663	41,5113
0,15094	1,007417	1506,35	0,0002686	41,4683

Table 27   Calculated data D-galactose at atmospheric pressure and 25°C.

molality, mol·kg^{-1}	$V_{\phi,2}$, cm^3·mol^{-1}	$K_{S,\phi,,2,\,prac}$·10^4, cm^{3}mol^{-1}bar^{-1}	$K_{T,\phi,2}$·10^4, cm^{3}mol^{-1}bar^{-1}	n_H±0,1
0,06346	110,36 (0,07)	-20,76 (0,38)	-16,92 (0,51)	8,61
0,10279	110,39 (0,04)	-20,32 (0,23)	-16,68 (0,35)	8,53
0,11873	110,41 (0,04)	-20,25 (0,20)	-16,66 (0,30)	8,50
0,15094	110,44 (0,03)	-19,95 (0,16)	-16,37 (0,24)	8,44

Table 28   Raw data for D-galactose at applied pressures

molality mol·kg⁻¹	p, bar	u, m·s⁻¹	γ	ρ, g·cm⁻³	$V_{\phi,2}$, cm³·mol⁻¹	$K_{S,\phi,2,prac.}$, cm³·mol⁻¹·bar⁻¹	$K_{T,\phi,2}$, cm³·mol⁻¹·bar⁻¹
0,06346	0,0	1500,80	1,01115	1,001454	110,36	-0,002076	-0,001693
	198,1	1534,02	1,01365	1,010162	110,67	-0,001753	-0,001395
	399,0	1567,73	1,01651	1,018641	110,92	-0,001476	-0,001141
	615,2	1603,93	1,01980	1,027397	111,14	-0,001215	-0,000902
	801,4	1634,96	1,02272	1,034646	111,29	-0,001018	-0,000722
	1009,9	1669,41	1,02599	1,042470	111,42	-0,000782	-0,000500
	1204,6	1701,34	1,02896	1,049516	111,50	-0,000612	-0,000342
	1391,3	1731,50	1,03165	1,056045	111,55	-0,000413	-0,000152
0,10279	0,0	1503,30	1,01147	1,004152	110,39	-0,002032	-0,001668
	198,9	1536,69	1,01398	1,012868	110,69	-0,001740	-0,001400
	401,9	1570,81	1,01687	1,021407	110,95	-0,001495	-0,001178
	605,6	1604,87	1,01997	1,029634	111,17	-0,001231	-0,000933
	801,6	1637,51	1,02304	1,037253	111,33	-0,001011	-0,000729
	1003,6	1670,87	1,02620	1,044817	111,46	-0,000798	-0,000530
	1199,3	1702,92	1,02919	1,051885	111,54	-0,000624	-0,000368
	1399,8	1735,35	1,03208	1,058878	111,60	-0,000455	-0,000209
0,11873	0,0	1504,32	1,01159	1,005236	110,41	-0,002025	-0,001666
	203,6	1538,54	1,01416	1,014143	110,72	-0,001741	-0,001407
	395,9	1570,80	1,01690	1,022223	110,97	-0,001477	-0,001163
	583,3	1602,20	1,01974	1,029805	111,17	-0,001262	-0,000967
	797,9	1637,89	1,02310	1,038158	111,35	-0,001004	-0,000725
	996,4	1670,73	1,02622	1,045590	111,48	-0,000813	-0,000549
	1197,2	1703,55	1,02928	1,052840	111,57	-0,000617	-0,000364
	1401,9	1736,67	1,03223	1,059972	111,63	-0,000455	-0,000213
0,15094	0,0	1506,35	1,01186	1,007417	110,44	-0,001995	-0,001638
	199,3	1539,83	1,01438	1,016119	110,74	-0,001709	-0,001375
	405,1	1574,38	1,01731	1,024742	110,99	-0,001442	-0,001130
	602,9	1607,45	1,02032	1,032703	111,19	-0,001201	-0,000908
	800,1	1640,20	1,02341	1,040347	111,35	-0,000966	-0,000688
	1007,1	1674,40	1,02665	1,048072	111,47	-0,000769	-0,000505
	1203,4	1706,47	1,02965	1,055138	111,56	-0,000586	-0,000334
	1400,1	1738,26	1,03248	1,061973	111,61	-0,000436	-0,000194

Table 29   Measured data for D-mannose at atmospheric pressure and 25°C

molality$\pm$0,0003, mol$\cdot$kg^{-1}	$\rho\pm4\cdot10^{-6}$, g$\cdot$cm^{-3}	u$\pm$0,07, m$\cdot$s^{-1}	$\alpha\pm5\cdot10^{-7}$, K^{-1}	$\sigma_p\pm$0,01, bar$\cdot$K^{-1}
0,07018	1,001844	1500,75	0,0002610	41,576
0,09728	1,003684	1502,32	0,0002625	41,540
0,11852	1,005124	1503,46	0,0002639	41,512
0,14992	1,007246	1505,37	0,0002660	41,470

Table 30   Calculated data D-mannose at atmospheric pressure and 25°C.

molality, mol$\cdot$kg^{-1}	$V_{\phi,2}$, cm$^3\cdot$mol^{-1}	$K_{S,\phi,2,\,prac}\cdot10^4$, cm^{3}mol^{-1}bar^{-1}	$K_{T,\phi,2}\cdot10^4$, cm^{3}mol^{-1}bar^{-1}	$n_H\pm$0,1
0,07018	111,41 (0,06)	-15,68 (0,60)	-13,01 (0,65)	8,04
0,09728	111,33 (0,04)	-15,70 (0,43)	-12,98 (0,47)	8,02
0,11852	111,25 (0,04)	-15,28 (0,35)	-12,48 (0,39)	7,94
0,14992	111,12 (0,03)	-15,74 (0,28)	-12,83 (0,31)	7,96

Table 31   Raw data for D-mannose at applied pressures

molality mol·kg^{-1}	p, bar	u, m·s^{-1}	γ	ρ, g·cm^{-3}	$V_{\phi,2}$, cm^3·mol^{-1}	$K_{S,\phi,2,prac.}$, cm^3·mol^{-1}·bar^{-1}	$K_{T,\phi,2}$, cm^3·mol^{-1}·bar^{-1}
0,07018	0,0	1500,75	1,01102	1,001844	111,41	-0,001568	-0,001301
	205,3	1535,21	1,01362	1,010862	111,65	-0,001306	-0,001057
	399,6	1567,82	1,01639	1,019055	111,84	-0,001086	-0,000852
	598,2	1601,10	1,01941	1,027106	111,99	-0,000897	-0,000677
	802,0	1634,98	1,02260	1,035055	112,10	-0,000644	-0,000434
	997,7	1667,47	1,02567	1,042407	112,18	-0,000538	-0,000339
	1198,4	1700,28	1,02873	1,049677	112,22	-0,000329	-0,000137
	1404,6	1733,57	1,03171	1,056884	112,23	-0,000133	0,000054
0,09728	0,0	1502,32	1,01121	1,003684	111,33	-0,001570	-0,001298
	205,3	1536,75	1,01381	1,012684	111,57	-0,001290	-0,001036
	399,6	1569,30	1,01658	1,020863	111,75	-0,001036	-0,000797
	598,2	1602,54	1,01959	1,028901	111,89	-0,000831	-0,000605
	802,0	1636,43	1,02279	1,036838	111,99	-0,000613	-0,000398
	997,7	1668,88	1,02586	1,044177	112,06	-0,000485	-0,000281
	1198,4	1701,83	1,02892	1,051436	112,10	-0,000357	-0,000161
	1404,6	1735,04	1,03189	1,058632	112,11	-0,000152	0,000038
0,11852	0,0	1503,46	1,01136	1,005124	111,25	-0,001528	-0,001248
	206,1	1538,09	1,01397	1,014146	111,48	-0,001282	-0,001020
	401,3	1570,85	1,01676	1,022349	111,66	-0,001061	-0,000815
	603,1	1604,58	1,01983	1,030499	111,80	-0,000835	-0,000604
	812,8	1639,52	1,02311	1,038641	111,91	-0,000649	-0,000431
	1002,6	1670,88	1,02609	1,045740	111,98	-0,000485	-0,000275
	1197,3	1702,77	1,02906	1,052772	112,02	-0,000342	-0,000141
	1394,6	1734,62	1,03191	1,059657	112,03	-0,000180	0,000015
0,14992	0,0	1505,37	1,01161	1,007246	111,12	-0,001574	-0,001283
	192,5	1537,71	1,01404	1,015666	111,35	-0,001335	-0,001062
	398,6	1572,26	1,01697	1,024322	111,54	-0,001084	-0,000828
	605,4	1606,83	1,02011	1,032658	111,69	-0,000859	-0,000618
	806,7	1640,25	1,02327	1,040461	111,80	-0,000647	-0,000418
	1004,1	1672,91	1,02636	1,047833	111,87	-0,000494	-0,000276
	1202,3	1705,40	1,02938	1,054977	111,91	-0,000357	-0,000148
	1402,0	1737,47	1,03226	1,061922	111,92	-0,000176	0,000026

Table 32 Measured data for D-ribose at atmospheric pressure and 25°C. Densities at 10, 20, 25 and 35 °C

molality $\pm 0,0003$, mol·kg^{-1}	$\rho \pm 4 \cdot 10^{-6}$, g·cm^{-3} 10°C	$\rho \pm 4 \cdot 10^{-6}$, g·cm^{-3} 20°C	$\rho \pm 4 \cdot 10^{-6}$, g·cm^{-3} 25°C	$\rho \pm 4 \cdot 10^{-6}$, g·cm^{-3} 35°C	$u \pm 0,07$, m·s^{-1}	α, K^{-1}	$\sigma_p \pm 0,01$, bar·K^{-1}
0,10200	1,005433	1,003838	1,002607	0,999525	1501,81	0,000265	41,5429
0,12008	1,006472	1,004852	1,003581	1,000508	1502,70	0,000267	41,5221
0,15331	1,008313	1,006665	1,005361	1,002283	1504,39	0,000269	41,4839
0,08543	1,004503	1,002929	1,001712	0,998639	1500,95	0,000264	41,5619
0,13315	1,007161	1,005536	1,004284	1,001197	-	0,000266	41,5071

Table 33 Calculated data D-ribose at atmospheric pressure and 25°C.

molality, mol·kg^{-1}	$V_{\phi,2}$, cm^3·mol^{-1}	$K_{S,\phi,2,\,prac} \cdot 10^4$, cm^{3}mol^{-1}bar^{-1}	$K_{T,\phi,2} \cdot 10^4$, cm^{3}mol^{-1}bar^{-1}	$n_H \pm 0,1$
0,10200	95,21 (0,04)	-12,12 (0,60)	-8,63 (0,65)	6,73
0,12008	95,21 (0,03)	-12,01 (0,43)	-8,44 (0,47)	6,70
0,15331	95,23 (0,03)	-12,03 (0,35)	-8,60 (0,39)	6,68
0,08543	95,20 (0,05)	-12,28 (0,28)	-8,86 (0,31)	6,66
0,13315	95,21 (0,03)	-	-	-

Table 34   Raw data for D-ribose at applied pressure.

molality mol·kg^{-1}	p, bar	u, m·s^{-1}	γ	ρ, g·cm^{-3}	$V_{\phi,2}$, cm^3·mol^{-1}	$K_{S,\phi,2,prac.}$, cm^3·mol^{-1}·bar^{-1}	$K_{T,\phi,2}$, cm^3·mol^{-1}·bar^{-1}
0,08543	0,0	1501,00	1,01125	1,001712	95,20	-0,001228	-0,000886
	200,8	1534,67	1,01379	1,010535	95,36	-0,000998	-0,000678
	413,0	1570,31	1,01682	1,019474	95,49	-0,000817	-0,000517
	609,5	1603,17	1,01982	1,027424	95,57	-0,000628	-0,000344
	814,0	1637,09	1,02302	1,035379	95,62	-0,000403	-0,000133
	1010,7	1669,62	1,02610	1,042752	95,64	-0,000269	-0,000011
	1215,9	1703,32	1,02923	1,050168	95,63	-0,000183	0,000062
	1408,2	1734,40	1,03199	1,056875	95,60	-0,000060	0,000177
0,10200	0,0	1501,81	1,01140	1,002607	95,21	-0,001212	-0,000863
	197,3	1534,99	1,01389	1,011271	95,37	-0,001041	-0,000715
	403,2	1569,49	1,01682	1,019948	95,49	-0,000819	-0,000512
	606,4	1603,42	1,01992	1,028168	95,58	-0,000607	-0,000317
	812,5	1637,76	1,02315	1,036186	95,63	-0,000457	-0,000182
	1006,1	1669,76	1,02618	1,043440	95,65	-0,000316	-0,000054
	1207,7	1702,80	1,02925	1,050729	95,65	-0,000192	0,000059
	1416,2	1736,42	1,03225	1,057997	95,62	-0,000038	0,000204
0,12008	0,0	1502,70	1,01157	1,003581	95,21	-0,001201	-0,000844
	200,8	1536,43	1,01411	1,012387	95,36	-0,001000	-0,000665
	413,0	1572,00	1,01714	1,021309	95,48	-0,000789	-0,000475
	609,5	1604,88	1,02014	1,029245	95,56	-0,000616	-0,000319
	814,0	1638,86	1,02334	1,037185	95,61	-0,000442	-0,000160
	1010,7	1671,29	1,02642	1,044545	95,63	-0,000280	-0,000011
	1215,9	1704,88	1,02954	1,051949	95,62	-0,000154	0,000103
	1408,2	1735,96	1,03230	1,058646	95,59	-0,000046	0,000202
0,15331	0,0	1504,39	1,01180	1,005361	95,23	-0,001203	-0,000860
	197,3	1537,44	1,01429	1,014000	95,37	-0,000974	-0,000652
	403,2	1571,96	1,01722	1,022653	95,49	-0,000771	-0,000468
	606,4	1605,85	1,02031	1,030851	95,56	-0,000572	-0,000286
	812,5	1640,20	1,02354	1,038848	95,61	-0,000431	-0,000160
	1006,1	1672,17	1,02657	1,046083	95,63	-0,000293	-0,000035
	1207,7	1705,20	1,02965	1,053354	95,63	-0,000180	0,000067
	1416,2	1738,74	1,03264	1,060605	95,60	-0,000033	0,000205

Table 35   Density data for L-arabinose at 20°C and 35°C.

molality, mol/kg	T=20°C		T=35°C	
	ρ, g/cm^3	$V_{\phi,2}$, cm^3/mol	ρ, g/cm^3	$V_{\phi,2}$, cm^3/mol
0,06960	1,002185	92,67	0,997905	94,38
0,10118	1,003966	92,74	0,999651	94,32
0,12582	1,005348	92,77	1,001006	94,29
0,15213	1,006813	92,82	1,002446	94,27

Table 36　Measured data for L-arabinose at atmospheric pressure and 25°C. Densities at 20, 25 and 35 °C

molality ±0,0003, mol·kg^{-1}	ρ±4·10^{-6}, g·cm^{-3} 20°C	ρ±4·10^{-6}, g·cm^{-3} 25°C	ρ±4·10^{-6}, g·cm^{-3} 35°C	u±0,07, m·s^{-1}	α±10^6, K^{-1}	σ$_p$±0,01, bar·K^{-1}
0,06960	1,002185	1,000982	0,997905	-	0,0002643	41,5429
0,10118	1,003966	1,002751	0,999651	1502,64	0,0002675	41,5221
0,12582	1,005348	1,004123	1,001006	1504,04	0,0002704	41,4839
0,15213	1,006813	1,005582	1,002446	1505,58	0,0002741	41,5619

Table 37　Calculated data L-arabinose at atmospheric pressure and 25°C.

molality, mol·kg^{-1}	$V_{\phi,2}$, cm^3·mol^{-1}	$K_{S,\phi,,2, prac} \cdot 10^4$, cm^{3}mol^{-1}bar^{-1}	$K_{T,\phi,2} \cdot 10^4$, cm^{3}mol^{-1}bar^{-1}	n_H±0,1
0,06960	93,35(0,04)	-	-	-
0,10118	93,35 (0,04)	-18,94 (0,41)	-14,53 (0,46)	7,44
0,12582	93,33 (0,03)	-18,61 (0,33)	-14,05 (0,37)	7,38
0,15213	93,34 (0,03)	-18,56 (0,27)	-13,70 (0,30)	7,36

Table 38　Raw data for L-arabinose at applied pressures

molality mol·kg^{-1}	p, bar	u, m·s^{-1}	γ	ρ, g·cm^{-3}	$V_{\phi,2}$,cm^3·mol^{-1}	$K_{S,\phi,2,prac.}$, cm^3·mol^{-1}·bar^{-1}	$K_{T,\phi,2}$, cm^3·mol^{-1}·bar^{-1}
0,10118	0,0	1502,64	1,01162	1,002751	93,33	-0,001894	-0,001453
	204,4	1536,97	1,01421	1,011713	93,61	-0,001628	-0,001217
	407,7	1571,01	1,01711	1,020263	93,83	-0,001349	-0,000964
	599,9	1603,12	1,02003	1,028035	93,99	-0,001112	-0,000748
	806,6	1637,49	1,02327	1,036079	94,13	-0,000886	-0,000543
	1010,8	1671,23	1,02647	1,043726	94,22	-0,000702	-0,000376
	1208,2	1703,56	1,02948	1,050856	94,28	-0,000545	-0,000235
	1409,4	1735,99	1,03237	1,057867	94,31	-0,000368	-0,000069
0,12582	0,0	1504,04	1,01192	1,004123	93,34	-0,001861	-0,001405
	182,8	1534,68	1,01421	1,012144	93,57	-0,001596	-0,001167
	396,0	1570,42	1,01723	1,021128	93,80	-0,001329	-0,000928
	610,1	1606,24	1,02049	1,029777	93,97	-0,001094	-0,000718
	809,9	1639,43	1,02362	1,037529	94,10	-0,000882	-0,000526
	1007,2	1672,00	1,02671	1,044907	94,18	-0,000701	-0,000363
	1204,5	1704,30	1,02972	1,052029	94,24	-0,000548	-0,000226
	1403,6	1736,45	1,03259	1,058963	94,27	-0,000399	-0,000091
0,15213	0,0	1505,58	1,01230	1,005582	93,34	-0,001856	-0,001370
	204,4	1539,87	1,01489	1,014516	93,59	-0,001578	-0,001124
	407,7	1573,91	1,01779	1,023040	93,79	-0,001315	-0,000889
	599,9	1605,99	1,02071	1,030789	93,95	-0,001090	-0,000688
	806,6	1640,37	1,02395	1,038810	94,07	-0,000884	-0,000505
	1011,0	1674,13	1,02716	1,046442	94,16	-0,000710	-0,000351
	1208,0	1706,34	1,03016	1,053538	94,21	-0,000551	-0,000209
	1409,4	1738,73	1,03305	1,060538	94,24	-0,000383	-0,000055